U.PORTO

MESTRADO

MEDICINA LEGAL

In vitro assessment of the effects of heroin on telomere length

Lina Solange Matos

M

2020

U.PORTO

Lina Solange Matos. *In vitro* assessment of the effects of heroin on telomere length

In vitro assessment of the effects of heroin on telomere length
Lina Solange Pereira Matos

INSTITUTO DE CIÊNCIAS BIOMÉDICAS ABEL SALAZAR

M.ICBAS 2020

Lina Solange Pereira Matos

In vitro assessment of the effects of heroin on telomere length

Dissertação de Candidatura ao grau de Mestre em Medicina Legal submetida ao Instituto de Ciências Biomédicas de Abel Salazar da Universidade do Porto.

Orientador– Doutor João Pedro Martins Soares de Castro e Silva
Categoria– Investigador Auxiliar
Afiliação- UCIBIO-REQUIMTE, Departamento de Ciências Biológicas, Laboratório de Toxicologia, Faculdade de Farmácia da Universidade do Porto
Coorientador- Professor Doutor Félix Dias Carvalho
Categoria– Professor Catedrático
Afiliação– Departamento de Ciências Biológicas, Laboratório de Toxicologia, Faculdade de Farmácia da Universidade do Porto

Cofinanciado por:
COMPETE 2020 PORTUGAL 2020 UNIÃO EUROPEIA Fundo Europeu de Desenvolvimento Regional

Agradecimentos

A escolha desta etapa foi tomada com todas as certezas de querer aprender e crescer profissionalmente, e estou orgulhosa de o ter acabado. Quero agradecer a todas as pessoas que contribuíram para que este projeto fosse possível.

Quero agradecer ao meu orientador, Doutor. João Pedro Silva, pela incansável e impecável orientação que me disponibilizou ao longo deste ano, assim como toda a aprendizagem que adquiri com os seus preciosos conhecimentos. Muito obrigada pelo apoio que me deu.

Muito obrigada ao Professor Doutor Félix Dias Carvalho, meu coorientador, pela valiosa orientação e pela confiança que depositou em mim quando escolhemos este projeto, que considero um importante desafio em que adorei trabalhar.

Ao Professor Ricardo Dinis Oliveira que nos cedeu gentilmente a diacetilmorfina para este projeto.

À Doutora Diana Silva e Mestre Rita Roque, pela ajuda e partilha de conhecimento, que contribuíram para a realização deste projeto.

Às técnicas de laboratório, aos colegas de doutoramento, investigadores e amigos que encontrei no laboratório, que me incentivaram. Com um carinho especial, à Telma Gomes, colega de laboratório que me ensinou muitos procedimentos, muito obrigada pela ajuda e paciência. À mestre Filipa Amaro que me deu uma força incondicional com o seu importante conhecimento, e pelo carinho de todos os dias.

Muito obrigada de coração às pessoas que tornaram este projeto possível com os seus esforços inestimáveis, aos meus pais, pois sem eles não passaria de um sonho. Ao meu namorado, que me ajudou incondicionalmente e me aturou todos os dias durante este processo com as minhas crises existenciais e acreditou em mim até ao fim. À minha irmã, que mesmo à distância, esteve sempre presente em todos os meus passos e me encorajou. A todos os meus familiares, amigos e colega de casa que me acompanharam neste caminho, que são pessoas muito especiais para mim.

Este trabalho foi financiado por Fundos FEDER através do Programa Operacional Competitividade e Internacionalização - COMPETE 2020 e por Fundos Nacionais (PIDDAC) através da FCT/MCTES no âmbito do projeto POCI-01-0145-FEDER-029584, assim como pela Unidade de Ciências Biomoleculares Aplicadas (UCIBIO), financiada através da FCT pelo projeto com a referência UIDB/04378/2020.

Abbreviations

BBB	Blood Brain Barrier
cAMP	3',5'-cyclic adenosine monophosphate
CNS	Central Nervous System
DA	Dopamine
DMSO	Dimethyl sulfoxide
Kb	Kilobases
DNA	Deoxyribonucleic Acid
EMCDDA	European Monitoring Center for Drugs and Drug Addiction
Flow-FISH	Flow-Quantitative Fluorescence In Situ Hybridization
GABA	*gamma*-Aminobutyric Acid
LAAM	Levo-Alpha-Acetylmethadol
LC	Locus Coeruleus
NAc	Nucleus Accumbens
NE	Noradrenaline
NSDUH	National Survey on Drug Use and Health
OR	Opioid receptor
PFC	Prefrontal Cortex
PNS	Peripheral Nervous System
POT1	Protection Of Telomeres 1
pre- PBC	Bötzinger complex
Q-FISH	Quantitative Fluorescence In Situ Hybridization
Q-PCR	Quantitative Polymerase Chain Reaction
RAP1	Repressor / Activator Protein 1
ROS	Reactive Oxygen Species
STELA	Single TElomere Length Analysis
TANKS1	Tankyrase 1
TD	Thiamine Deficiency
TERRA	Telomeric repeat-containing RNAs
TeSLA	Telomere Shortest Length Assay
TIN2	Interacting protein 2
TL	Telomere Length
TPP1	Tripeptidyl Peptidase 1
TRF	Terminal Restriction Fragment
TRF1	Telomere Repeat-binding protein 1
TRF2	Telomere Repeat-binding protein 2
U-STELA	Universal STELA
VTA	Ventral Tegmental Area
WHO	World Health Organization

INDEX

FIGURE INDEX

TABLE INDEX

Abstract

Heroin use is a worldwide public health concern, being associated with acute and chronic diseases, accelerated aging, and early death. Telomeres play a crucial role in maintaining the body's normal function, and their shortening is a strong aging biomarker. Until today, the mechanisms involved in the accelerated aging process, especially on telomere function after heroin use, remain unclear. This work thus aimed at establishing a protocol to assess *in vitro* effects of heroin on telomere length of neurons, and determine such effects, contributing to understand the risks of heroin use.

SH-SY5Y neuroblastoma cells were subcultured at 1:3 or 1:10 split ratios and proliferation rates were assessed using the sulforhodamine B (SRB) assay at regular passages to determine the number of subcultivations and/or time required for these cells to reach a decline phase. This cell line was selected for having a short doubling time (about 27 h) and for expressing the μ and δ opioid receptors. Metabolic activity and cell membrane integrity of SH-SY5Y cells, exposed to 1 nM - 100 µM heroin (3,6-diacetylmorphine) for 24h, were assessed using the MTT reduction and lactate dehydrogenase (LDH) release assays, respectively. Absolute telomere length was determined by qPCR after every other day administrations of 1 nM and 1 µM heroin for 3 and 6 days (2 and 3 additions, respectively). Exposure to 1 µM XAV939, a tankyrase 1 (TNKS1) inhibitor, which has been reported to reduce telomere length at this concentration, for 72 hours, was used as a positive control.

The proliferation rates of SH-SY5Y cells split at a 1:3 ratio were lower after passage 30, suggesting that cells at this passage could be entering the decline phase of proliferation. Heroin did not affect the metabolic activity or membrane integrity of SH-SH5Y cells up to 100 µM. Also, none of the heroin concentrations tested significantly affected telomere length after 3 or 6 days of exposure. Telomere length in 1 nM heroin-treated cells after 3 days was 1900 ± 989 kb/telomere, while in vehicle and baseline controls telomeres measured 3600 ± 875 kb/telomere. Ate the 1 µM concentration, there was no change in the telomeres length when compared to the control. Telomere length after XAV939 treatment was 2300 ± 762 kb/telomere, compared to 3100 ± 873 kb/telomere in the vehicle control. However, contrary to what was expected, these values were not significantly different. However, the number of independent experiments was limited due to the Covid-19 pandemic-related lockdown.

Overall, the data obtained suggested that heroin does not shorten telomeres up to 6 days of exposure. However, it is plausible that longer periods of heroin treatment would be required to observe any statistically significant results. As such, further research is required to clarify the involvement of heroin in the regulation of telomere length.

Keywords: 3,6-diacetylmorphine, opioids, absolute telomere length, cellular senescence, accelerated aging.

Resumo

O consumo da heroína é um problema de saúde pública global, estando associado a doenças agudas e crónicas, envelhecimento acelerado e morte precoce. Os telómeros desempenham um papel crucial para manter a homeostasia das funções biológicas e o seu encurtamento é um forte biomarcador de envelhecimento. Até hoje, os mecanismos envolvidos no processo de envelhecimento acelerado, principalmente na função dos telómeros após o uso de heroína, permanecem desconhecidos. Assim, este trabalho teve como objetivo estabelecer um protocolo e avaliar os efeitos *in vitro* da heroína no comprimento dos telómeros em células neuronais, contribuindo para a maior compreensão dos riscos associados ao uso da heroína.

As células de neuroblastoma SH-SY5Y foram semeadas com rácios de divisão de 1:3 ou 1:10 e as taxas de proliferação foram avaliadas usando o ensaio da sulforhodamina B (SRB) a passagens regulares, para determinar o número de divisões e/ou o tempo necessário para estas células atingirem uma fase de declínio da proliferação. Esta linha celular foi selecionada devido ao seu tempo de duplicação curto (cerca de 27 h) e por expressar os recetores opióides μ e δ. A atividade metabólica e a integridade da membrana celular de células SH-SY5Y expostas a 1 nM - 100 µM de heroína (3,6-diacetilmorfina) por 24 horas foram avaliadas usando os ensaios de redução de MTT e libertação da lactato desidrogenase (LDH), respetivamente. O comprimento absoluto dos telómeros foi determinado por qPCR após administrações em dias alternados de 1 nM e 1 µM de heroína por 3 e 6 dias (2 e 3 adições, respetivamente). A exposição a 1 µM de XAV939, um inibidor da tankyrase 1 (TNKS1), que foi comprovado na redução do comprimento dos telómeros nesta concentração, por 72 horas, foi usada como um controle positivo.

As taxas de proliferação de células SH-SY5Y divididas na proporção de 1:3 foram menores após a passagem 30, sugerindo que as células nesta passagem poderiam estar a entrar na fase de declínio da proliferação. A heroína não afetou a atividade metabólica ou a integridade da membrana das células SH-SH5Y até 100 µM. Além disso, nenhuma das concentrações de heroína testadas afetou significativamente o comprimento dos telómeros após 3 ou 6 dias de exposição. De notar, o comprimento dos telómeros em células tratadas com 1 nM heroína após 3 dias foi de 1900 ± 989 kb/telómero, enquanto no veículo e controlos basais dos telómeros mediram 3600 ± 875 kb/telómero. O comprimento dos telómeros após o tratamento com XAV939 foi de 2300 ± 762 kb/telómero, em comparação com 3100 ± 873 kb/telómero no controlo com o veículo. Porém, ao contrário do que era esperado, estes valores não foram significativamente diferentes. No entanto, o número de experiências independentes foi limitado devido ao encerramento do Laboratório relacionado à pandemia de Covid-19.

De um modo geral, os dados obtidos sugeriram que a heroína não encurta o comprimento dos telómeros até 6 dias de exposição. No entanto, é plausível que períodos mais longos de tratamento com heroína sejam necessários para observar efeitos estatisticamente significativos a este nível. Como tal, será necessário continuar esta investigação para esclarecer o envolvimento da heroína na regulação do comprimento dos telómeros.

Palavras-chave: 3,6-diacetilmorfina, opióides, comprimento absoluto de telómeros, senescência celular, envelhecimento precoce.

1. Introduction

Illicit drug use contributes to major health problems and may lead to early death, representing a high burden for public health, society, and economy. Most recent data (2017) from the United Nations Office on Drugs and Crime (UNODC) reported 585,000 drug-related deaths worldwide. Moreover, around 35 million individuals had disorders related to drug abuse, of which nearly 13% required treatments for dependency (UNODC, 2019). Specifically, 0.6% of the global population aged between 15-64 was reported to be opioid-addicted. The same data from the 2017 UNODC report revealed that in North America (including USA and Canada), 110,000 out of 167,000 (66%) of drug-related deaths were due to opioid use (EMCDDA, 2019; UNODC, 2019; Wang, 2019). According to the European Monitoring Center for Drugs and Drug Addiction (EMCDDA), opioids (e.g. heroin) are involved, in average, in eight to nine out of every 10 drug-induced deaths reported in Europe (UNODC, 2019). In Portugal, the number of deaths attributed to illicit drugs, in a population aged 15–64, decreased in 2016 compared to 2015 (from 55 to 30, respectively), and the majority of deaths occurred in males. Noteworthy, 39% of all drug-related treatments performed in Portugal during 2015 targeted heroin consumers (EMCDDA, 2019).

Misuse of synthetic opioids further represents an ongoing challenge. For example, over 51,000 overdoses related to fentanyl were reported in the US and Canada in 2017, while Tramadol seizures in North, West, and Central Africa increased from 10 Kg in 2010 to nearly 125 tons in 2017 (UNODC, 2019).

Acknowledging the long-term adverse effects of opioids to the brain could potentially lead to improved therapeutics for chronic opioid users, as well as to the implementation of more effective prevention policies.

1.1. Opioids

Opioids belong to the analgesic class of drugs, being mostly used in the treatment of chronic pain, including the one observed in different types of cancer, and in post-surgery settings. Their analgesic effect may be attributed to their binding to pain receptors, also known as nociceptors, which are distributed all over the body and are composed by several nerve cells that detect a chemical, thermal, or mechanical stimulation. However, opioids have also been used recreationally, being the most widely consumed and lethal drugs of abuse (Martinez and Ballesteros, 2019; Schaefer et al., 2017; Stein, 2016).

Opioids comprise both endogenous and exogenous ligands. There are four groups of endogenous ligands: β-endorphins, enkephalins, dynorphins and the nociception/orphanin FQ (N/OFQ) peptide, produced within the body to inhibit the response

to pain. These can be released by immune cells, acting for example at sites of infection, and by neurons in the central nervous system (CNS). Exogenous opioids may be semi-synthetic (chemically modified from natural opioids), including heroin, hydrocodone, and oxycodone; synthetic, comprising fully chemically synthesized opioids, which include fentanyl, methadone and pethidine (Corder et al., 2018; Stein, 2016; Zollner and Stein, 2007); and plant-derived: opioids like morphine, thebaine, and codeine, which are present in the opium extracted from the plant *Papaver somniferum L.* (opium poppy) through the plant's capsule opening. Of note, thebaine and codeine are only found in the mature capsule, at late stages of the plant growth (Martinez and Ballesteros, 2019; Schaefer et al., 2017; Stein, 2016).

The main differences among opioids lie in their chemical structure, pharmacokinetics, and physicochemical properties. However, they share the affinity for the mu Opioid Receptor (μ-OR) (Corder et al., 2018). Opioids may be divided into three distinct groups, according to their chemical structure: opioids containing an 4,5-epoxymophinan ring (e.g. morphine, codeine, oxymorphone, oxycodone, buprenorphine, hydromorphone, hydrocodone), phenylpiperidines (e.g. alfentanil, fentanyl, sufentanyl) and diphenylheptylamines (e.g. methadone) (Drewes et al., 2013).

Opioids may be administered through the intravenous, oral, nasal, anal or intrathecal routes, according to the desired action. The main purpose of intravenous or epidural injection, for example, is to have the opioid action on the peripheral nervous system (PNS), being the CNS-related effects almost negligible (e.g. respiratory depression is null). Most important, the choice of the administration route influences how fast the opioids act. For example, opioids act quicker following intravenous administration than after other types of administration. In addition, bioavailability of opioids following oral administration is only about 25 % (Schaefer et al., 2017; Zollner and Stein, 2007).

The absorption, metabolism and excretion also differ among opioids. Absorption of these substances depends on the desired effect and target. For example, loperamide and diphenoxylate show reduced effects on the CNS, being mostly absorbed in the intestine and thus being mostly used for diarrhea treatment (Schaefer et al., 2017; Zollner and Stein, 2007). However, each group is cleaved by a specific enzyme: for example, the 4,5-epoxymophinan ring is mainly cleaved by CYP2D6 (Cytochrome P450 2D6) and phenylpiperidines by CYP3A4. The CYP3A4 isoform is probably the enzyme most involved in diphenylheptylamines' metabolism. However, the CYP2B6, CYP2D6 and CYP2B19 isoforms are likely to be involved as well. Of note, some opioids (e.g. morphine, oxycodone, hydromorphone, methadone, ketobemidone, tramadol, tapentadol, fentanyl, sufentanil, buprenorphine and codeine) are usually not orally administered, since they present a high gastrointestinal permeability (Corder et al., 2018; Drewes et al., 2013).

The diverse opioids have different affinities for each opioid receptor. For example, fentanyl, hydromorphone, methadone, morphine and tapentadol have a higher affinity for μ-OR, compared to codeine, oxycodone, tilidine and tramadol. Moreover, oxycodone and morphine have affinity for the kappa (κ) opioid receptor (κ -OR), being this affinity higher for oxycodone compared to morphine (Drewes et al., 2013). The metabolism of opioids depends on the administration route, but remains poorly studied (Hutchinson, 2002). The metabolism also depends on the gender, age, health, disease state, genetic factors and concomitant use of medications. The first step of opioids' metabolism occurs in the liver and the excretion is mainly processed by the kidneys (Trescot et al., 2008).

Opioid-related dependence induced by their use in chronic pain treatment is an increasing concern. However, there are distinct opinions regarding the theory that people become addicted to opioids after being treated to relieve chronic pain through the prescription of opioids. Kolodny et al. (2015) associated the use of opioids for chronic pain treatment with deaths caused by opioids' overdose, mostly as a result of overprescription. Of note, the National Survey on Drug Use and Health (NSDUH) reported that 4 out of 5 opioid addicts became addicted after treatment for chronic pain relief (Muhuri, 2013). Also, most of such addicts have turned to illicit opioids, since replacement of legal opioids by heroin, for example, is cheaper, further leading to increased mortality (Kolodny et al., 2015). However, Gardner et al. (2011) showed that the probability of addiction after opioid treatment is low, since in animal models chronic pain inhibits: 1) the circuit of the brain responsible for reward/relapse, thus removing the craving sensation, decreasing dopamine levels (these are usually increased following opioids use), and 2) the development of physical dependence stimulated by opiates. A temporary opioid treatment causes minor side effects. However, the risk for addiction increases for longer treatment periods (Kiyatkin, 2019).

The prevention of opioid addiction derived from non-medical prescription also represents a major concern. Non-medical prescription is the use of opioids that are liable to be prescribed by the doctor for chronic treatment, but in an inappropriate way by family relatives who have easy access to these medicines. University students represent the main social group using opioids obtained through non-medical prescriptions. In particular, the students lacking knowledge on opioids are 9.6 times more likely to use non-medical opioids prescriptions than the students who know the risks of unattended opioid use (Kolodny et al., 2015).

1.2. Heroin

Heroin, also known as 3,6-diacetylmorphine, is a highly potent opioid, with analgesic properties. Its recreational use is widespread, representing a major public health concern (Banta-Green et al., 2017; Barrio et al., 2013). Among heroin users, overdose is the main cause of mortality, along with infections. Three of the main risk factors for heroin overdose include 1) the administration by injection, which provides a fast and intense effect, and 2) the concomitant extra-medical use of pharmaceutical opioids (e.g. methadone, fentanyl) along heroin use, and 3) a recorded history of problems related to substance use. In fact, the use of methadone (an OR agonist) or buprenorphine (a modulator of ORs) in replacement therapy may increase the probability of overdose in the first two weeks of treatment if individuals continue to use heroin during the treatment (Roxburgh et al., 2019).

Heroin can be used in many ways, including injection, smoking, or sniffing (Gutowicz et al., 2006). Injection is the mostly used method by addicted individuals, due to the orgasmic-like feeling produced during administration. Heroin levels in the blood disappear faster after intravenous administration and become undetectable in 10-40 minutes. This change in plasma heroin levels can be accentuated when using other medications, like as the ones used in HIV treatment. Also, heroin addicts are usually poly-drug users. Moreover, intravenous heroin further aggravates the public health problems, due to the elevated number of infections (e.g. with HIV and/or Hepatitis C Virus) as a result of syringe sharing (Barrio et al., 2013; Buttner, 2000; Gutowicz et al., 2006).

In the brain, heroin mainly suppresses pain sensation and decreases anxiety, and may possibly lead to a state of happiness and euphoria (Banta-Green et al., 2017; Barrio et al., 2013; Buttner, 2000). On the other hand, the main adverse effects of heroin consumption are more evident in the brain and include neuronal loss, ischemic neuronal damage, development of infectious disease (e.g. meningitis). Noteworthy, these disorders may develop into a chronic disease and/or result in early death (Buttner, 2000).

The effects of heroin in the brain of chronic abusers has been analyzed by imaging exams, having infections been identified as the main cause of neuropathologic changes. In fact, the immune system is usually depressed in these individuals, leading for example to meningitis and ventriculitis. In addition, lymphocytic meningitis may occur when these individuals are at an early phase of HIV. Inhalation of heroin powder, filled with impurities, may cause a spongiform leukoencephalopathy, which in the initial stage is characterized by cerebellar ataxia, soft speech, and motor restlessness. In individuals injecting and sniffing heroin, the globus pallidus (subcortical structure of the brain) may develop necrotic injuries, which may cause the impairment of motor functions (Kiyatkin, 2019). Also, heroin may affect the cerebellum, thus possibly affecting motor functions. The use of heroin has been described to decrease grey matter and blood flow, with the consequent decline in cognitive functions, inhibitory controls, reflection impulsivity and the connection between different

parts of the cerebellum (Moreno-Rius, 2019). Moreover, cerebral edema was observed in 90% of deaths by heroin overdose. Of note, opiate addiction does not seem associated with μ-ORs' density reduction or heroin's binding affinity (Buttner, 2000; Gutowicz et al., 2006).

Heroin has a fast action in the brain, due to its high liposolubility, which allows it to permeate the blood-brain barrier (BBB). However, only a small amount of heroin reaches the brain. In addition, heroin has a very low affinity for the μ-OR. The metabolism of heroin is summarized in Figure 1. The deacetylation of heroin into 6-Monoacetylmorphine (6-AM) by hydrolysis, which is a fast process, takes place in the blood, allowing 6-AM to cross the BBB more easily than heroin. Hence, 6-AM is found in the brain and in blood flow at higher concentrations compared with heroin (Dinis-Oliveira, 2019; Rook, 2006).

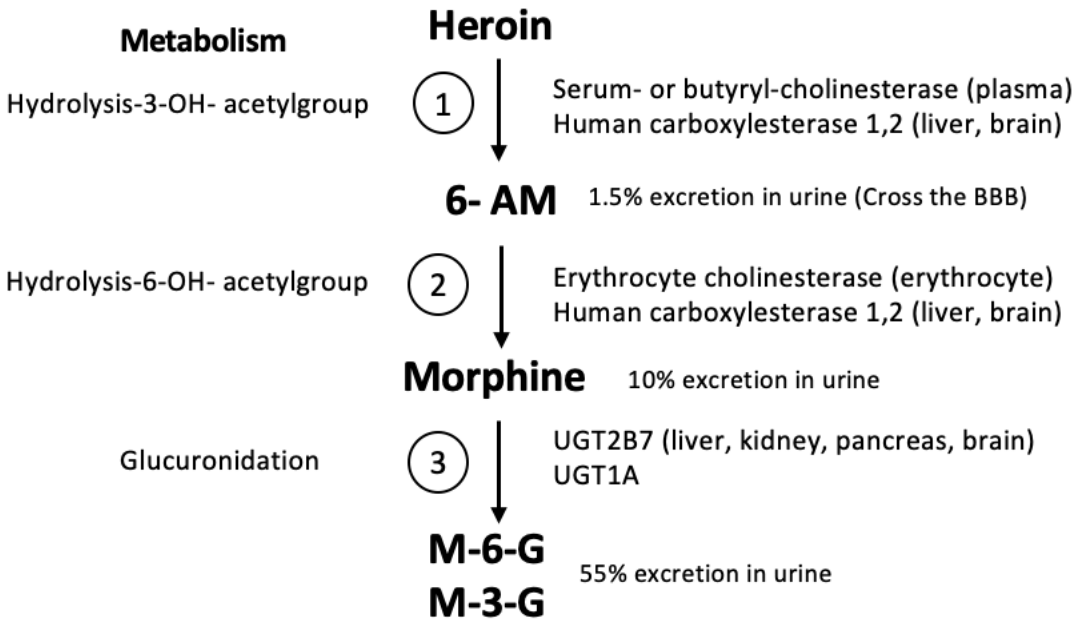

Figure 1. Heroin metabolism. Esterases are distributed throughout several tissues and blood. The enzymes responsible for the hydrolysis of heroin are serum- or butyryl-cholinesterase, found in plasma, and human carboxylesterase 1,2, in liver and brain. Erythrocyte cholinesterase, located in erythrocytes, and human carboxylesterase-1,2 convert 6-AM into morphine. The glucuronidation of morphine to Morphine-6-Gluronide(M-6-G) and Morphine-3-Gluronide(M-3-G) is mediated by UGT2B7 and UGT1A. These metabolites are hydrophilic metabolites mostly excreted by urine, and a small percentage in bile. Adapted from Rook et al. (2006).

The enzymes responsible for heroin metabolism are serum- or butiylryl-cholinesterases, present in the plasma, and the human carboxylesterase-1,2, found in the liver and brain. Erythrocyte cholinesterase, located in erythrocytes, and human carboxylesterase-1,2 convert 6-AM into morphine, which is able to bind with high affinity to the μ, k and δ ORs. Morphine may be further transformed into M-6-G and M-3-G in a process catalyzed by uridine 5´-diphosphateglucuronosyltransferases (UGT) subtypes UGT2B7 and UGT1A, which are synthesized in the gut and found in the liver, kidney, pancreas and brain. After

an intravenous heroin administration, morphine can be detected up to 12 h in the blood and until 24 h in the urine, 71 % being excreted by urine. 6-AM can be detected between 1-3 hours in plasma and between 1.2-4.3 hours in urine. The highest concentrations of morphine, as a metabolite of heroin, can be detected between 3.6-8.0 minutes following heroin administration (Dinis-Oliveira, 2019; Rook, 2006). Upon oral and rectal administration, neither heroin nor 6-AM are found in plasma. Also, heroin is rapidly hydrolyzed to morphine in the colon or duodenum, before absorption (Rook, 2006). When the heroin is inhaled, the degradation takes place in the intranasal mucous and the lung. Degradation via this route is faster, since heroin is rapidly absorbed by mucous membranes due to its lipophilicity (Trescot et al., 2008). Gottås et al, showed that after heroin intravenous injection, the heroin levels in the blood flow and brain decrease while the 6-AM values measured in both places are higher, reaching higher concentrations than heroin. The maximum concentration of 6-AM reported by the authors was 4 times higher compared with heroin, and 7 times higher than morphine (Gottås et al., 2013).

The determination of heroin-related deaths remains a challenge for toxicologists in forensic medicine. 3,6-diacetylmorphine has a half-life of approximately 5 minutes in the plasma, being converted into 6-AM with a half-life in blood of about 20-30 minutes. Moreover, 70 % of the intravenously administered heroin is eliminated in the urine after being metabolized. M3G and M6G are the heroin metabolites mainly found in urine (55%), followed by morphine (10%) and 6-AM (1.5%). Blood, teeth, hair, semen, urine and nails comprise the main matrices to detect heroin in an individual (Thaulow et al., 2018). Considering the different concentrations and time points at which heroin may be detected in each of these matrices, their analysis is thus important to determine the time between drug intake and death or even to discern the opioid that led to death. Establishing heroin overdose as a cause of death can be hard when the consumers use other substances along heroin. For example, codeine (an opiate with weaker analgesic effects compared to heroin) is a metabolite of heroin but it can also be used as every day's medication. The distinction between codeine intake and codeine as a heroin's metabolite thus relies on that heroin's administration also produces a metabolite named 6-acetylcodeine that is usually found at low concentrations in urine. The presence of this metabolite thus indicates that the codeine detected is a result of heroin use. 6-AM may be rapidly degraded, thus its detection in the blood of an individual's corpse may represent the result of a fast death, while its detection in another matrix like the vitreous humor or urine signifies that death occurred much later after heroin administration. Morphine concentrations in the blood are higher when the interval between intake and death are small. The morphine/codeine ratio can be measured in peripheral blood in post-mortem situations. A morphine/codeine ratio higher than 1 it indicates the presence of heroin, while a ratio lower than 1 indicates that codeine is present

(Rook, 2006; Thaulow et al., 2018). In fact, Thaulow et al. concluded that this ratio could be used to accurately determine the relation of morphine/codeine in cardiac blood, peripheral blood, skeletal muscle, and pericardial liquid. However, the use of this ratio in humor vitreous samples was less precise (Thaulow et al., 2018).

1.3. Opioids' mechanisms of action

Opioids bind to ORs, which belong to the family of G protein-coupled receptors (GPCRs), which are in turn composed of seven α-helical transmembrane domains. The binding of opioids to ORs is schematized in Figure 2.

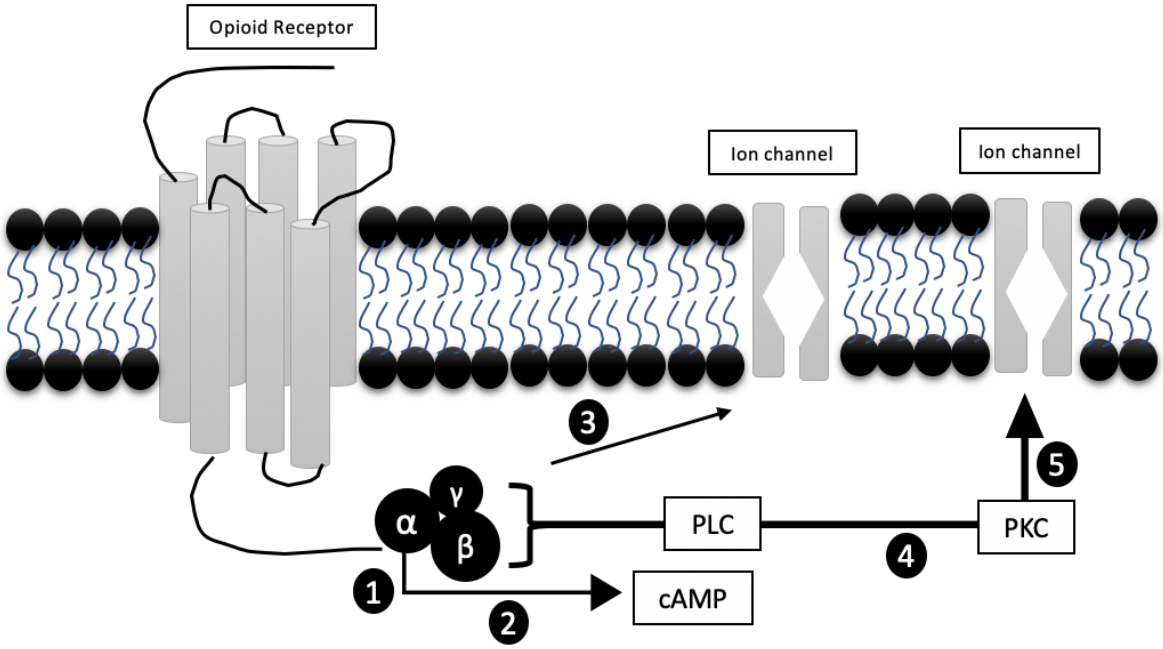

Figure 2. Opioid Receptor signalling. Opioid Receptors are G protein-coupled receptors, comprising subunits α, β and γ attached to the OR transmembrane domains. **1)** Binding of opioids to the receptor leads to the division of G protein subunits G_{α} and $G_{\beta\gamma}$. **2)** G_{α} leads to adenyl cyclase inhibition, triggering the blocking of cAMP synthesis; **3)** while $G_{\beta\gamma}$ decreases the conductance of voltage-gated Ca2+ channels, and/or **4)** activates the phospholipase C and phosphokinase C pathway leading to **5)** Ca^{2+} channels opening, which further results in hyperpolarization (the feeling of pain ceases to exist) (Corder et al., 2018; Zollner and Stein, 2007). Adapted from Zollner and Stein (2007).

GPCRs comprise three subunits, α, β and γ, attached to the OR transmembrane domains. The opioids' signals are blocked by adenosine diphosphate (ADP), which in turn inactivates the G protein. The endogenous or exogenous opioids bind to the ORs and, upon this binding, the trimeric G protein complex gets disconnected into two subunits, Gα and Gβγ, which trigger distinct pathways. Gα leads to adenyl cyclase inhibition, and subsequently inhibits 3',5'-cyclic adenosine monophosphate (cAMP) synthesis. Noteworthy, cAMP, a secondary messenger, has many functions, mostly related to

neurotransmitter release, opening and closing of ion channels, receptor sensitivity and receptor internalization. Opioid-induced cAMP inhibition results in decreased cAMP, as well as potassium and calcium levels in the presynaptic neurons, which become hyperpolarized (Stein, 2016; Williams et al., 2001). In turn, the Gβγ subunit interacts with ion channels in the presynaptic neuron, blocking the opening of voltage-gated calcium channels located in the cell membrane, thus preventing ion release. However, in the postsynaptic neuron, upon opioid binding, the subunit Gβγ binds to and causes potassium channels to open, leading to an increased potassium release, which prevents the formation of the action potential (Weis and Kobilka, 2018; Williams et al., 2001).

ORs are activated in response to pain and by different substances, including opioids, nicotine, and alcohol. There are three main ORs, mu (μ), delta (δ) and kappa (κ), but opioids bind with more selectivity to the μ-OR, which are scattered throughout the body. They may be found in the CNS, mostly in the cortex, thalamus, hippocampus, locus coeruleus (LC), ventral tegmental area (VTA), nucleus accumbens (NAc), as well as in the PNS, within the cranial and spinal nerves, and in the amygdala, in interneurons (Feltenstein and See, 2008; Kosten and George, 2002; Luethi and Liechti, 2020; Zollner and Stein, 2007).

Opioids work closely together with other regulatory mechanisms important to maintain body homeostasis. For example, when ORs are chronically exposed to morphine, during pain treatment, the synthesis of the endogenous opioid β-endorphin becomes atrophied, as a result of not being required anymore. Upon morphine withdrawal, the endogenous system is dysregulated, not only the β-endorphin synthesis but also the weaker pain signaling, resulting in ineffective pain relief. Hence, opioids are used to treat addiction provoked by pain treatment until there is a recovery from the decompensation of the body homeostasis. There are other factors that have been reported to contribute to the dysregulation of the opioid system, including depression and other psychologic disorders, Alzheimer's disease, personality disorders, and exposure to addictive drugs (Emery and Akil, 2020).

Binding of opioids to ORs in the brain is mainly processed through the mesolimbic pathway, also known as the reward pathway, which is one of the dopaminergic pathways in the brain, linking the VTA, sited in the midbrain, to the ventral striatum of the basal ganglia (located in the forebrain). The mesolimbic pathway is a part of the brain responsible for motivation and sensation of pleasure, being also involved in the generation of the addiction phenomenon (Kosten and George, 2002). The NAc receives dopaminergic impulses from the VTA. NAc is located in the anterior part of the brain responsible for pleasure, motivation, and maternal behavior, besides being a center of the reward circuit. Its activation causes the feeling of euphoria/happiness. Of note, drugs that have the ability to create addiction lead to increased dopamine (DA) levels and act, indirectly or directly, in dopaminergic neurons at the VTA (Volkow et al., 2019). Dopaminergic neurons are tightly controlled by

GABA interneurons, which also contain ORs. As such, opioid binding to GABA interneurons leads to the inhibition of GABA release. Following this blockade, dopamine activates the reward pathway to induce pleasure (Gardner, 2011; Volkow et al., 2019). After repeated opioids use, the association between pleasure and opioid use, usually designated by Drug Linking, is formed (Williams et al., 2001).

Different thermal, chemical and mechanical stimuli may activate the circuit to respond to pain. The stimuli may travel through a sensory axon to the dorsal horn in the spinal cord through a positive charge called Action Potential (AP), or travel between neurons, releasing inhibitory or excitatory neurotransmitters (e.g. GABA, glutamate), and activating their respective receptors (Figure 3) (Stein, 2016).

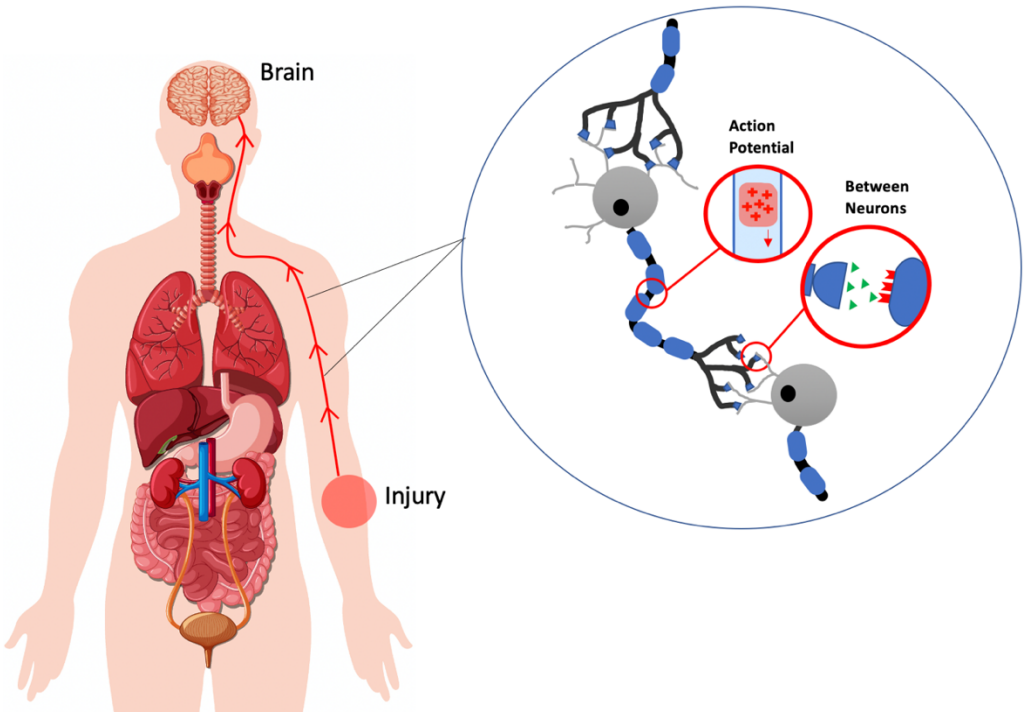

Figure 3. The different types of signal travel through neurons. As pain signals reach the brain, these may follow two distinct pathways: 1) the stimuli may travel through a sensory axon to the dorsal horn in the spinal cord through an Action Potential, or through synaptic signalling between neurons, releasing inhibitory or excitatory neurotransmitters (e.g. GABA, glutamate). Adapted from (Medicurio, 2018).

When an AP travels through a neuron up to the presynaptic neuron, the voltage-gated calcium channels open, allowing the entrance of calcium ions. Consequently, glutamate (excitatory neurotransmitters) vesicles fuse to the membrane of the presynaptic neuron and glutamate gets released into the synaptic cleft. In the postsynaptic neurons, glutamate binds to glutamate receptors, enabling the positively charged ions (e.g. sodium) to enter in the post-synaptic neuron, thus causing neuronal depolarization. This depolarization generates

a new AP, and the signal keeps on moving. This process is called excitatory signaling. On the other hand, during inhibitory signaling an AP increases the positive charge in the presynaptic neuron, opening voltage-gated calcium channels and allowing the influx of calcium ions. Calcium ions then cause the release of vesicles containing GABA (inhibitory neurotransmitters) into the synapse. GABA binds to the GABA receptors, resulting in the entry of negatively-charged ions (e.g. chloride), producing a hyperpolarization that blocks the sodium channel, and terminating the AP (the signal stops) (Stein, 2016; Williams et al., 2001).

1.4. Analgesic effects of opioids

There are two main pain signaling pathways: the ascending pathway, which sends a signal to the brain when an external stimulus provokes pain; and the descending pathway, which sends information from the brain to turn off the ascending pathway and stop the information of injury, thus relieving the sensation of pain in the damage location (Williams et al., 2001). These pathways are summarized in Figure 4.

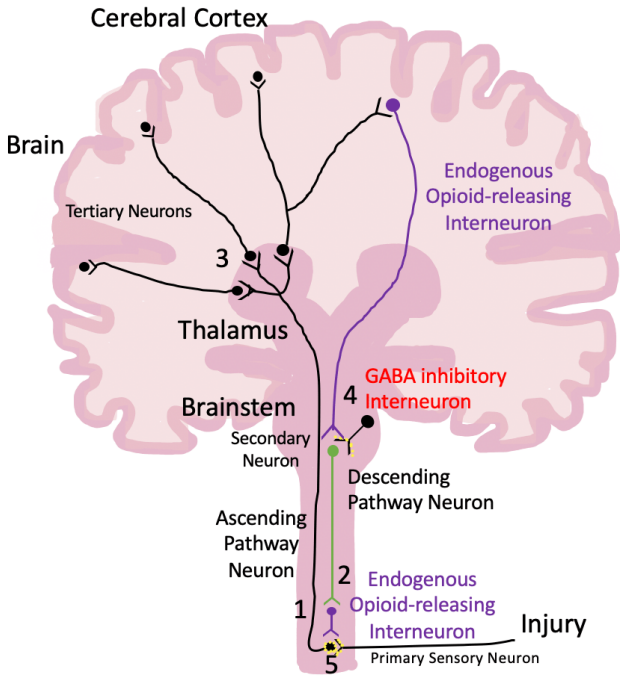

Figure 4. Ascending and descending pathways of pain control. The ascending pathway (1) sends the signal to the brain when an injury occurs while the descending pathway (2) has the function to respond, to control the pain and how serious it is, through the endogenous opioids released. (3) Tertiary neurons; (4) Endogenous opioid-releasing interneuron; (5) synaptic cleft for inactivation of the ascending pathway. Adapted from (Medicurio, 2018).

In response to an injury (e.g. hurting a finger), primary neurons send the injury information to the brainstem through the spinal cord up to the thalamus, which processes the sensory information. Then, the secondary neurons contact with tertiary neurons (number 2 in Fig. 4), which activate other regions of the brain cortex allowing giving us the meaning/perception of the pain. This information is important to induce the body to produce natural painkillers (endogenous opioids), that is, depending on the pain level that it is felt, the hypophysis synthesizes endorphins, enkephalins, and dynorphins to control the discomfort caused by ache. These endogenous opioids then bind to the ORs, blocking the release of GABA vesicles, maintaining the AP and activating the descending pathway (number 4). Neurons usually signal the activation of opioid-releasing interneurons in the spinal cord. However, as the release of endogenous opioids inhibits pre- and postsynaptic signaling, causing the communication between primary and secondary neurons to fail, the blockade of the ascending pathway becomes required (number 5 in Fig. 4). To stop pain perception, hence the synthesis of endogenous opioids, GABA inactivates the descending pathway, stopping the action potential and causing hyperpolarization that signals the ascending pathway to stop (Gardner, 2011). With the ascending pathway turned off, the brain stops receiving information and pain perception stops. Similarly to endogenous opioids, exogenous opioids stop the signal transmission to the spinal cord (number 1 in Fig. 4) by binding to the ORs on this site (Gardner, 2011; Williams et al., 2001).

1.5. Side effects, Dependence and Tolerance of opioids

Control of severe pain through the use of opioids still represents a hard assignment due to the many adverse effects it carries on. In fact, both the therapeutical and recreational use of opioids have side effects, even in acute exposure conditions (Kiyatkin, 2019). In general, concerning the nervous system, opioids cause adverse symptoms such as euphoria, sedation and coma. In addition, these substances may induce hypotension and bradycardia, which may further lead to respiratory depression (Del Vecchio et al., 2017; Wang, 2019).

The effects at the respiratory system are also triggered by the μ- and δ- ORs, whose activation causes respiratory depression through the inactivation of the pre-Bötzinger complex, a group of nerves located in the brain that controls the respiratory system. The inhibition of this complex further results in hypercarbia, hypoxia, and at high opioid doses, apnea may also occur (Manzke et al., 2003).

Opioids stimulate nausea and vomiting, as they may activate chemoreceptors in the postrema, which are located in the brain stem (Miller and Leslie, 1994). The activity of this brain area is increased mainly when people are in movement, due to the action of the

vestibular system, which is responsible for maintaining equilibrium (Zollner and Stein, 2007). Binding of opioids to ORs present throughout the gastrointestinal system inhibits intestinal secretions due to the stimulation of tonic contraction of the smooth muscle, increasing water absorption from the intestine and causing obstipation. These consequences are especially concerning for cancer patients, who can become tolerant to opioid treatment (Farmer et al., 2018; Zollner and Stein, 2007).

The release of histamine from mast cells is another result from using opioids, contributing to exaggerated allergic reactions, such as urticaria, and other symptoms like hypotension and tachycardia (Barke and Hough, 1993; Zollner and Stein, 2007).

Upon a chronic use of opioids, tolerance, as well as physical and psychosocial dependency may develop. Tolerance and dependency comprise two different concepts: tolerance relates to the requirement of higher dosages compared to the previous ones to produce the same effect, while dependency is associated with the drug craving sensation following a drug's withdrawal (Christie, 2008; Kosten and George, 2002). Of note, the total mechanisms associated with opioid tolerance and dependency remains ambiguous.

In general, although the NAc is the core of the reward circuit, the reward center works sequentially connecting the VTA, NAc, and ventral pallidum regions through the medial forebrain bundle, a neural pathway with a set of fibers that connect parts of the brain that depend on each other. The dopaminergic neurons in the VTA project neurons to the amygdala and hippocampus that mediate emotional and memory associations to the prefrontal cortex (PFC), along with addiction-related stress and self-regulation (Gardner, 2011; Volkow et al., 2019; Zollner and Stein, 2007).

cAMP signaling is one of the main mechanisms contributing to tolerance. cAMP signaling follows three stages: upon opioid use, the neuronal levels of this secondary messenger decrease, and the cells start working to replace cAMP loss. This replacement, set to anticipate a decline in cAMP levels, turns neurons into an overactive state. In this sense, the cells get prepared for the next time opioid consumption occurs, so that cAMP homeostasis is maintained. As a result, in the ensuing opioid use, higher opioid doses will be necessary to put the neurons back to a normal state. However, if the opioid administration does not occur while the neurons are overactive, withdrawal symptoms like anxiety, panic and excessive sweating start appearing (Williams et al., 2001). Of note, withdrawal symptoms are associated with the overactivation of neurons mainly located in 3 areas of the body: VTA, locus coeruleus (LC) and gut. The LC is located in the brainstem and it is mainly involved in the response to stress and panic (Kosten and George, 2002). It activates the sympathetic nervous system, causing sweating, pupil dilation and increased heart and breathing rate. Following opioid consumption, the neurons in the LC, which contain ORs, become hyperpolarized, leading the LC to act in an opposite mode to its

normal function, causing sleepiness/drowsiness, sedation, skin dryness, breathing and heart rate decrease, and pupil constriction. As these neurons become tolerant after the administration of some opioid doses, the withdrawal symptoms become visible, with the LC triggering jittery, anxiety, panic, excessive sweating, mydriasis (dilated pupils) and extremely rapid heart and breathing rate. In the gut, certain neurons maintain the normal gut function, i.e. the movements to push contents out. Hence, constipation is the consequence of opioids use in the gut. During withdrawal, the absorption of water is decreased, inducing diarrhoea (Kosten and George, 2002; Williams et al., 2001). GABA inhibitory interneurons, which keep the dopaminergic neurons into the VTA, also get tolerant to opioids, replacing the usual feeling of happiness and euphoria by a sensation of discomfort. To prevent this situation, addicted individuals usually use opioids again and in larger amounts (Williams et al., 2001). After repeated use, 1) the body associates opioid use to pleasure, 2) pre-emptive cAMP increase leads to tolerance, and 3) withdrawal symptoms often discourage the individual from stopping opioid use. However, if the individual does not use opioids over a few weeks, the withdrawal symptoms start fading away, although this is usually a very hard and painful process (Emery and Akil, 2020; Williams et al., 2001).

The cerebellum is linked to drugs addiction and has more neurons compared with the encephalon, its important role in the consumption of illicit drugs being already demonstrated (Moreno-Rius, 2019). The use of opioids changes the synthesis of the molecules in the brain, altering the normal function of the brain. For example, after an acute opioid administration, thiamine levels increase, indicating a degenerative process, that causes neuronal loss. Glucose levels in the cerebellum have also been reported to decline as a result of morphine use (Moreno-Rius, 2019). The repetitive heroin exposure modifies the proprieties of aminoamides vesicles (e.g. serotonin and catecholamine), suggesting neurotransmission deregulation (Buttner, 2000; Moreno-Rius, 2019).

1.6. Effects of heroin consumption

The main consequences of heroin use are more evident in the brain and include neuronal loss, ischemic neuronal damage, and development of infectious disease (e.g. meningitis). These disorders, which arise mostly from sharing non-sterile syringes and are a consequence of a compromised immune system, may develop into a chronic disease and/or result in early death (Buttner, 2000; Gutowicz et al., 2006). Also, as previously mentioned, the presence of brain infections has already been identified as the main cause of neuropathologic changes (Sato et al., 1979; Shirley Y. Hill and Michael A. Mikhael, 1979).

The brain requires a constant access to oxygen to maintain its normal functioning. However, respiratory depression, which may occur following heroin or fentanyl use, is a common effect of all μ-OR agonists, which may lead to acute brain hypoxia and ultimately to coma. Opioid-induced hypoxia causes necrotic lesions in the brain, neuronal loss on globus pallidus (subcortical structure of the brain), impairment of mental and motor functions, and hypodensities in the basal ganglia, similarly to carbon monoxide intoxication. Of note, in some cases the lesions caused are worse following the use of adulterated substances (Buttner, 2000). Solis et al. studied hypoxia and hypothermia in the rat brain following heroin and fentanyl exposure, as well as fentanyl contaminated by heroin and vice-versa. The oxygen values were measured by sensors, the drugs were injected according to a specific timeline, and the use of heroin, fentanyl and the heroin-fentanyl mixtures were used alternately. The study was divided in two parts: in the first one, the rats were administered the drugs, and their effects on the temperature in the NAc, temporal muscle, and skin, as well as on the rats' locomotor activity were assessed; and in the other part, extracellular levels of oxygen in the NAc were measured after administration of the drugs in the same conditions (Solis et al., 2017). Both fentanyl and heroin cause a decrease in oxygen levels in the NAc. The mixtures of heroin and fentanyl induced a more prolonged decrease in oxygen levels. However, the drop-in oxygen induced by fentanyl was faster than that of heroin. Fentanyl and heroin produced relatively similar decreases in oxygen NAc, suggesting that fentanyl is 20 times stronger than heroin in its ability to induce cerebral hypoxia. These differences between drugs in the dynamics of the oxygen response may be related to their known differences in pharmacokinetics (Solis et al., 2017; Solis et al., 2018).

Hill et al. diagnosed cerebral atrophy, significantly small sulci, and larger than normal ventricle in the brains of chronic heroin addicted individuals, using Computerized Trans-axial Tomography (Hill and Michael A. Mikhael, 1979). Heroin may also affect the cerebellum, thus possibly affecting motor functions. The use of heroin has been described to decrease gray matter and blood flow, with the consequent decline in cognitive functions, inhibitory controls, reflection impulsivity and the connection between different parts of the cerebellum (Moreno-Rius, 2019). Autopsies performed to the corpses of chronically addicted individuals (confirmed through the loss of nerve cells in the gray matter located in the hippocampus) demonstrated that cerebral edema with weight gain occurred in 90% of the cases analyzed. Moreover, in 10-15 % of cases, necrosis and brain injuries were identified (Buttner, 2000; Gutowicz et al., 2006).

1.7. Treatment of opioid addiction

One of the main effects of opioid overdose is respiratory depression. In normal conditions, once breathing is reduced, there is an increase in carbon dioxide and a decrease in oxygen levels, leading the central and peripheral neurons' chemoreceptors, which detect these changes, to emit the required signals to increase breathing rates. However, in the presence of extremely high doses of opioids, the neurons remain in fatigue mode, preventing the brain from sending the signals to restart breathing. This situation may be circumvented by the injection of naloxone, an antagonist of ORs with a similar chemistry formulation to morphine. Naloxone binds to the ORs with more affinity than opioids, activating the neurons and restarting breathing (Luethi and Liechti, 2020; Roxburgh et al., 2019; Zhang et al., 2018; Zollner and Stein, 2007).

Nowadays there is a treatment for opioid addiction comprising various agonists of ORs. However, each case needs to be specifically evaluated to select the most adequate opioid for a successful recovery. Administration of methadone, an OR agonist whose effects last for a few days, is the most used treatment (Kosten and George, 2002). Methadone acts mostly on the μ-OR but the dependence caused during recovery is minimal, and the tolerance is reduced. Treatment with methadone has shown good results and proves to be effective, as it reduces relapse rates, hormone synthesis, and improves social behavior. Normally, individuals leave the recovery with methadone after 2 years in average, although some need to be treated for life. Levo-Alpha-Acetylmethadol (LAAM), a synthetic opioid similar to methadone, is also used and, like methadone, it has the same behavior as illicit opioids when it binds to the μ-OR, but the LAAM's action lasts longer. However, LAAM has not been used due to its dangerous secondary effects, which include heart problems. Naltrexone is also used, mainly immediately after the detoxified from other addicted opioids. It binds with 100 times more affinity to the μ-OR compared with opioids. Upon binding of naltrexone to the ORs in the brain, this OR agonist stimulates the reward system, avoiding relapse, by inactivating the synthesis of noradrenaline, which is associated with withdrawal symptoms. Noteworthy, binding of naltrexone to ORs does not cause the feeling of euphoria often related to opioid drugs use, so it does not encourage the addicted individuals to use opioids (Kosten and George, 2002). Buprenorphine binds to the μ-OR and when used in high doses it inactivates the ORs, triggering withdrawal. Buprenorphine is safer than methadone for treatments that are followed at home, since high doses of methadone may lead to overdose, unlike the high doses of buprenorphine. Moreover, buprenorphine prevents binding of other opioids to the ORs and blocks itself when high doses are detected. The control of buprenorphine dosages is crucial for treatment success, since low doses act

similarly to methadone and high doses produce effects similar to naltrexone (Kolodny et al., 2015; Kosten and George, 2002).

1.8. Telomeres

Telomeres are repetitive TTTAGGG nucleotide sequences located at the linear chromosome ends, with approximately 10-15 kilobases (kb), which provide protection against DNA damage (Giardini et al., 2014; Lu et al., 2013).

These structures play an important role when transcription is active by preventing the fusion among the remaining chromosomes. Telomeres are composed of double-stranded DNA that ends in a single strand, protected by T-Loop. One of the strands, the G-strand, is guanine-rich, which allows the development of the G-quadruplex (a secondary structure comprising four guanines linked by hydrogen bonds in helical shape that form a square planar structure called G-quartet, stabilized by a cation in the center) to create a D-Loop. The other strand, named C-strand, is rich in cytosine, producing a T-Loop due to this strand's invasion of G-quadruplex. These two loops work together to prevent the occurrence of loose ends in the linear chromosome (Figure 5A and 5B) (Giardini et al., 2014; Lu et al., 2013; Songyang, 2017).

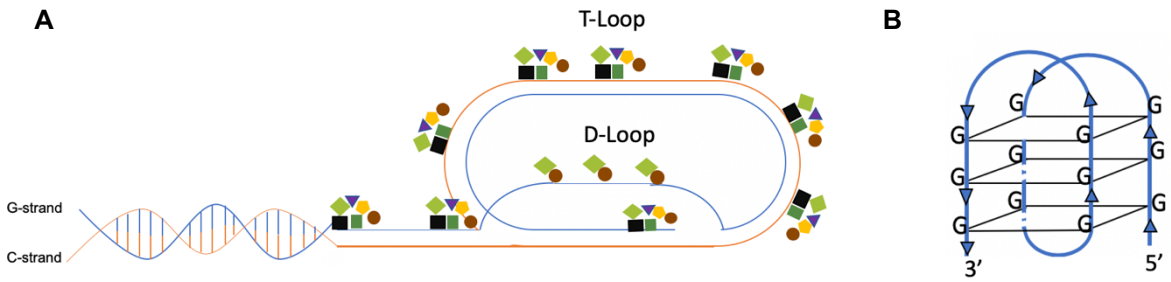

Figure 5. D-loop and T-loop formation. A) The synthesis of T-Loop and D-Loop are a protection against DNA damage in cell division and prevent fusion with chromosome neighbors. **B)** G-quadruplex is made with G-quartets that are hydrogen-bonded to create the D-Loop, preventing the DNA from getting loose ends. Adapted from (Giardini et al., 2014; Martinez and Blasco, 2015).

The telomeric DNA is replicated in each cellular division, with telomerase playing a key role in telomere synthesis. This enzyme is a ribonucleoprotein that contains a template to elongate telomere length (TL) by adding a hexanucleotide (TTAGGG) sequence, and it is composed by a telomerase reverse transcriptase (TERT) and a telomerase RNA component (TERC). TERC expression is ubiquitous, while telomerases and TERT expression is very low in somatic cells (Lu et al., 2013; Srinivas et al., 2020). Telomerases are highly expressed in the brain during the embryonic stage, but their expression decreases after birth, except in stem cells, keratinocytes and activated lymphocytes, which maintain high telomerase levels. The expression and activity of TERT occur mostly in the

adult brain, especially in the hippocampus, olfactory bulb, and subventricular zone, since these regions have an increased density of neuronal progenitor cells (Fathi et al., 2019; Liu et al., 2018). Noteworthy, telomerase malfunction is often found in degenerative diseases, and in most cancers. Of note, telomere length may vary according to the type of cancer. For example, long telomeres are usually found in cancers like lung adenocarcinoma, neuroblastoma, bladder cancer, melanoma, testicular germ-cell cancer, kidney and endometrial cancer, while telomeres are often shorter in pancreatic cancer (Campa et al., 2019; Srinivas et al., 2020).

Telomeres adopt exclusive structures to support various telomere-binding proteins, like the Shelterin Complex (also called Telosome Complex), which protect them from DNA repair mechanisms. This complex consists of 6 proteins (Figure 6): telomere repeat-binding protein 1 and 2 (TRF1 and TRF2), the TRF1-interacting protein 2 (TIN2), Repressor / Activator Protein 1 (RAP1), Protection Of Telomeres 1 (POT1) and Tripeptidyl Peptidase 1 (TPP1, a protein associated with POT1) (Lu et al., 2013).

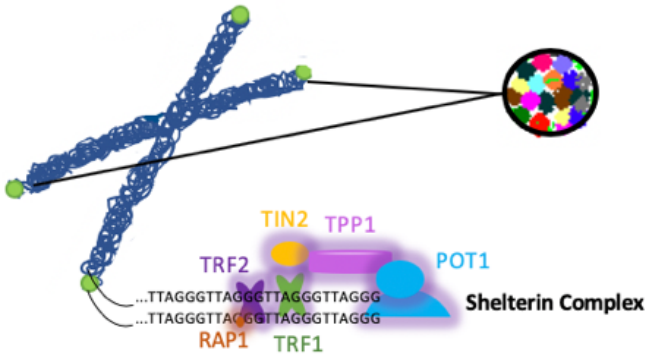

Figure 6. The Shelterin complex. The main structure that protects and regulates the mechanism in each replication is constituted by 6 proteins that in each cellular division works to synthesize the telomeres. Adapted from Shay and Wright (2019).

These proteins play specific roles and work jointly to protect and regulate the telomeres function. TRF1 is an inhibitor of telomerase activity, limiting the telomere length. It plays a crucial role in length control, since the lack of regulation of TL may lead to cell apoptosis. In fact, Lu et al. found that the lack of TRF1 in mice resulted in increased apoptosis during the embryonic stage (Lu et al., 2013). TRF2 protects the T-Loop from being recognized as a DNA break and acts as a negative regulator of TL. The overexpression of TRF2 promotes telomere shortening, while the loss of TRF2 leads to the extinction of the T-Loop, triggering the activation of p53, and ultimately apoptotic cell death. Of note, both TRF1 and TRF2 promote DNA replication. POT1 helps in the formation of the D-Loop and it is associated

with TPP1, a protein responsible for maintaining telomerase activity. Separation of POT1 and TPP1 leads to the deregulation of the shelterin complex (Lu et al., 2013; Srinivas et al., 2020).

There is a subtelomeric region at the end of the telomeres consisting of noncoding telomeric repeat-containing RNAs (TERRA), which is present in most cell types. TERRA is mostly active when telomeres are short. In turn, in long telomeres, TERRA works together with the shelterin complex to prevent the telomerase-mediated addition of hexanucleotides to telomeres (Azzalin and Lingner, 2015; Srinivas et al., 2020).

Cells lose the capacity to divide over time due to the inability of DNA polymerase to replicate the terminal ends of the chromosomes, leading to a loss of the Shelterin complex's ability to bind the T-loop, which ultimately results in exposed telomere ends. This process, which naturally occurs as a result of cellular aging, is commonly defined as cellular senescence, and is often associated with the absence of telomerase. The senescence state represents the last and permanent state of the cell, known as the Hayflick limit (Magalhaes and Passos, 2018; Victorelli and Passos, 2017), in honor of Leonard Hayflick. This researcher observed that specific human diploid cell strains WI-26, WI-38 and WI-44 had a division limit of 50 times and that when this limit was reached, cells lost their ability to divide (Hayflick, 1965). Basically, senescence represents a safety mechanism that forces cell division to stop. If it were not for this mechanism, uncontrolled cell division would continue, with concomitant accumulation of irreversible errors, as it occurs in cancer cells, for example. Senescence affects different organs and tissues, being associated with several pathologies, such as atherosclerosis or neurodegenerative diseases (Calcinotto et al., 2019).

The main reason for senescence to occur is the decrease in telomere length. Telomere length can be affected by environmental factors, inflammation, oxidative stress, different pathologies (e.g. Alzheimer's disease, inflamed liver, chronic hepatitis, liver cirrhosis) (Arsenis, 2017; Barnes et al., 2019; Hirota, 1999) and lifestyle (e.g. obesity, drug abuse, smoking, sedentarism) and/or psychological stress (Srinivas et al., 2020).

By comparing telomere length in the peripheral blood from women with crack cocaine (the crystalized format of cocaine) addiction with a group control of elderly women, Levandowski et al. showed that these substances contributed to telomere shortening (Levandowski et al., 2016). Grun et al. (2018) studied the relation between obesity, which is known to reduce life span, and telomere length, in particular the role played by the shelterin complex in obesity. The authors observed an increased expression of shelterin complex elements, mainly TRF1, in obese people, compared with the control group, and the telomere length was higher in the healthy control group compared to moderate and morbidly obese. The authors suggested that the upregulation of TRF1 could be due to the

augmented adipose tissue, causing oxidative stress, which in turn leads to telomeric DNA damage (Frohnert et al., 2011; Grun et al., 2018). Savale et al. analyzed the evolution of the aging process in a group of Chronic Obstructive Pulmonary Disease patients, a group of smokers with no respiratory diseases, and a control group of healthy non-smokers. The authors examined cytokine concentrations and measure the telomeres in leukocytes of blood samples collected from each group, concluding that telomere shortening was visible in circulating leukocytes in Chronic obstructive pulmonary disease compared with smokers without lung disease (Savale et al., 2009).

Obstructive apnea sleep (OAS) is a disorder in which episodes of complete or partial obstruction of the upper airway occur during sleep. Patients with OAS have been reported to have a decrease in telomere length, compared with healthy individuals (Savolainen et al., 2014). TL was measured in leukocytes present in the blood samples collected from 1964 participants with a mean age of 61.5 years. The authors further suggested that oxidative stress and high inflammation levels were the main link between OAS and telomere length decrease.

Of note, mitochondrial dysfunction and subsequent increase in oxidative stress seem to play a major contribution to cellular senescence and telomere shortening. Reactive oxygen and nitrogen species (ROS/RNS) may oxidize pyrimidines and purines in the DNA chain, which in turn are likely to induce errors in telomeric DNA (Barnes et al., 2019).

1.9. Drugs of Abuse and telomere shortening

Accelerated aging represents one of the several adverse effects of drug use (Vakonaki, 2019). In this context, telomere shortening appears to be a suitable marker to assess such accelerated aging following prolonged drug abuse. Between the ages of 18 and 76, telomeres lose, in average, 27 base pairs (bp) per year. Several studies have already identified that telomere length decreases due to increased oxidative stress produced by polydrug exposure (Bachi et al., 2017; Cheng et al., 2013; Valdes et al., 2005; Yang et al., 2013). In fact, Yang et al. showed that oxidative stress declines telomerase activity, and cell proliferation. Moreover, Hemann et al. reached similar conclusions and further showed that such decreased telomerase activity may ultimately lead to cell apoptosis (Hemann et al., 2001; Yang et al., 2013).

Vakonaki et al. (2019) compared telomere length in individuals concomitantly abusing different drugs (e.g. heavy cannabis, amphetamines, benzodiazepines, opiates, and cocaine) with a control group comprising healthy individuals, noticing a significant decrease in the length of telomeres from drug abusers. Also, the authors found that the biological age in those individuals was higher than chronologic age, indicating premature aging. As such,

the authors further concluded that the accumulated use of drugs over time plays a crucial role in telomere shortening since the telomeres seemed to be shorter in users with longer consumption habits.

Binge drinking also precipitates the aging process. Moreover, the toxicological consequences of alcohol depend on the time of exposure and on the acetaldehyde levels in the blood, as acetaldehyde triggers carcinogenic effects in the upper respiratory tract (Martins de Carvalho et al., 2019; Yamaki et al., 2019). Yamaki et al. measured the size of telomeres in leukocytes of men with alcohol dependency, observing that these individuals had shorter telomeres than the individuals in the healthy control. The authors suggested that the metabolism of alcohol (i.e. conversion of ethanol in acetaldehyde) results in an excessive production of ROS that interact with the cells' mechanisms of defense and in DNA replication, inducing breaks in the DNA chain (Yamaki et al., 2019).

Tobacco, in addition to being associated with the onset of chronic diseases, is also associated with premature aging. Cigarette smoking causes an accumulation of oxidative stress and inflammation leading to premature death. The decrease in telomere length of leukocytes from smokers compared with non-smokers has already been reported (Bateson et al., 2019; Khan et al., 2019). Moreover, by analyzing leukocytes in the blood samples collected from female smokers, Valdes et al. (2005) observed that cigarette smoking represented a major risk factor for premature aging. In fact, the authors observed that, when compared to non-smokers, smokers or ex-smokers appeared to be approximately 4.6 years older.

Khan et al., (2019) analyzed the role played by several factors associated with cigarette smoking (e.g. smoking status, smoking intensity, type of filter, second-hand smoke, serum cotinine levels) in telomere length. The authors observed that heavy smokers (i.e. individuals who smoked more cigarettes per day) had shorter telomeres due to increased systemic inflammation, which was likely related to the suppression of proinflammatory responses. The same study also showed that tobacco-induced telomere shortening was associated with increased oxidative stress levels that resulted in DNA damage (López-Flores et al., 2017).

In particular, to date, the effects of heroin in the mechanisms underlying the regulation of telomere length remain mostly unknown. Cheng et al. analyzed the connection between heroin use and aging, by measuring telomerase activity in peripheral blood samples, and assessing cerebral function with magnetic resonance imaging (MRI). The authors observed that the telomerase activity was lower in heroin users compared to a control group (non-heroin users), suggesting premature aging (Cheng et al., 2013). The authors further noted that changes in telomerase activity caused loss of integrity of the right dorsal prefrontal cortex, the brain area related to addiction, as indicated by modifications in the connectivity

between the right dorsal prefrontal cortex and regions responsible for aging. Yang et al. also reported a reduction in the length of telomeres in leukocytes from blood samples collected from heroin consumers (Yang et al., 2013). By assessing a possible association between the method of consumption (i.e. intravenous, olfactory or smoked) and the size of the telomeres, the authors showed that telomeres were longer in the leukocytes of heroin addicts that inhaled heroin as a preferential method. These studies further showed that leukocytes represent an interesting model to easily assess the effects of a substance on telomeres length. However, it should be noted that after metabolization heroin also targets other organs and matrices (e.g. brain). However, to the best of our knowledge, there is no published data regarding the effects of heroin in telomeres from such organs or matrices.

1.10. Measurement of Telomeres Length

To date, there are several methods used to measure telomeres, including quantitative polymerase chain reaction (qPCR), terminal restriction fragment (TRF) analysis, a variety of quantitative fluorescence in situ hybridization (Q-FISH) methods, flow-quantitative FISH (Flow-FISH), single telomere length analysis (STELA) and telomere shortest length assay (TeSLA) (Lai et al., 2018).

TRF analysis measure the length of telomeres through Southern-blot. Briefly, TRF consist of the digestion of the genomic DNA preserving the telomeric DNA with a restriction enzyme. Restriction enzymes degrade genomic DNA while maintaining the sequences of telomeres intact because these do not have sites liable to the action of restriction enzymes. Subsequently, telomeric sequences are detected by Southern blot, with the length of telomeres calculated by comparing its position in the agarose gel with a DNA ladder of known weights. The main disadvantages of this method rely in the difficulty to detect very short telomeres (<2kb), along with being quite time-consuming (Lai et al., 2018; Mender and Shay, 2015).

Q-FISH is based on fluorescent microscopy and evaluate the chromosomes metaphasic or interphase nuclei, using a peptide nucleic acid probe, which undergoes hybridization and binds to the required target (telomere sequence) after being measured with a fluorescence detector. The fluorescence signal intensity is proportional to the size of telomeres. This method has a high sensitivity to short telomeres, allowing the measurement of telomeres with less than 0.1 kb of telomeric repeats. However, this procedure requires cells to be in the mitotic phase, thus preventing its use in studies involving senescent cells (Canela et al., 2007; Lai et al., 2018).

Flow-FISH is a method similar to Q-FISH, established to improve Q-FISH by reducing the time required to prepare the target cells and the duration of the flow cytometry step,

providing the fluorescence of telomeres in interphasic cells. The main disadvantage is the high frequency of inaccurate quantifications due to the binding of sequences that are located away from the chromosomal ends (Lai et al., 2018).

Single telomere length analysis (STELA) is a procedure that combines Southern-Blot with PCR. This technique allows the detection of telomeres in senescent cells, as well as the measurement of telomeres below 8 kb in length with high precision. To resolve the main limitation of STELA, which is the detection of subsets of individual chromosome ends, another method, Universal STELA (U-STELA) may be used. However, this alternative method is only able to measure telomeres over 8 kb (Lai et al., 2018; Lai et al., 2017).

Telomere shortest length assay (TeSLA) was developed as an improvement to the methods mentioned above, displaying a detection threshold ranging from below 1 kb to approximately 18 kb. Its main advantages include its high sensitivity and requirement for only small DNA amounts. Moreover, complementary post-analysis processing may include DNA separation by Southern-blot and the use of fast-processing software. However, this method usually needs to be performed by skilled and trained researchers (Lai et al., 2018; Lai et al., 2017).

qPCR thus emerges as an adequate alternative to measure telomere length due to its easiness and speed and mostly due to the requirement of only small DNA amounts. This method allows two types of telomere quantification: relative telomere length, in which the length of telomeres in each sample is calculated relatively to a template of a single copy gene (SCG), allowing to calculate the Telomere/Single Copy Gene (T/S) ratio, proportional to the average of telomere length in kb pairs; and absolute telomere length (aTL), by interpolating the size of the telomeres in a given sample from a standard curve designed using standards with known size of telomeric repeats (Cawthon, 2009; O'Callaghan and Fenech, 2011).

The main advantages and limitations of each method are summarized in Table 1.

Table 1. Comparison between the different methods for measuring the length of telomeres.

Method	Advantages	Limitations	References
TRF	Cancer cells' compatibility; Fast protocol.	Telomeres < 2Kb are undetectable; Hight DNA quantities.	(Lai et al., 2018; Mender and Shay, 2015)
qPCR	Easy and fast procedure; Low amounts of DNA required. Possibility to determine absolute telomere length.	Cannot be used in cancer research (unable to measure telomere length in aneuploid cells);	(Cawthon, 2009; Lai et al., 2018; O'Callaghan and Fenech, 2011)
Q-FISH	High sensibility for short telomeres (until < 0.1); Used to cells and fixed cells.	Only cells in mitotic phase; Difficult protocol.	(Canela et al., 2007; Lai et al., 2018)
Flow-FISH	Faster than Q-FISH.	False negatives with similar telomeres sequences.	(Lai et al., 2018)
U-STELA	Detects short telomeres; Precision.	Labor-intensive protocol; Only reads telomeres above 8 kb.	(Lai et al., 2018; Lai et al., 2017)
TeSLA	Sensitive and accurate;	Needs experience.	(Lai et al., 2018; Lai et al., 2017)

The types of samples used are essential to measure telomere length. Leukocytes from peripheral blood are usually the most suitable type of sample. Indeed, leukocytes allow having a higher DNA quantity and quality, which is essential to obtain reliable required results for the analysis of telomeres. However, other matrices are commonly used to evaluate the length of telomeres, such as saliva and blood stains. Although obtaining these matrices requires less invasive procedures, the quality of the DNA obtained is lower (Stout et al., 2017)

2. Objectives

Telomeres are important structures protecting chromosomes from degradation. Their loss of integrity may result in genomic instability, faster cell senescence and ultimately cell death. In fact, there are studies that associate telomere shortening with aging and dementia, for example. Heroin use is linked to a short lifespan and to the onset of chronic diseases, but the mechanisms of action involved in such effects remain poorly understood. Moreover, there is no information regarding its effects on cells other than leukocytes. Thereby, it becomes important to assess if heroin affects telomere length, in particular in neuronal cells, considering these are the main targets of heroin's action.

Here, we hypothesized that prolonged heroin administration may affect telomere length. In this sense, we outlined two specific objectives:

1) Establish a protocol to adequately assess telomere length following heroin administration;
2) Evaluate the effects of heroin on the length of the telomeres in an SH-SY5Y cell model.

We expect that our findings will contribute to better understand the physiological changes occurring in heroin consumers and possibly identify additional risk factors associated with heroin use, thus contributing to improve therapeutic approaches to heroin addicts.

3. Materials and Methods

3.1. Chemicals

Antibiotic/antimycotic solution (10 000 U mL^{-1} penicillin, 10.00 mg mL^{-1} streptomycin, 25.00 µg mL^{-1} amphotericin B) was obtained from Grisp (Porto, Portugal). Heat-inactivated fetal bovine serum (FBS), 0.25% trypsin/EDTA, and Hank's balanced salt solution (HBSS) were acquired from Gibco Laboratories (Lenexa, KS, USA). All other reagents used in this work were purchased from Sigma Aldrich (St. Louis, MO, USA), unless stated otherwise.

3.1.1. Diacetylmorphine

Heroin (3,6-Diacetylmorphine) (LIPOmedical, Arlesheim, Switzerland) was kindly provided by Prof. Ricardo Dinis-Oliveira (CESPU, Gandra, Portugal) in its hydrochloride format.

Diacetylmorphine was dissolved in phosphate buffer pH=5 (65.9 mM, monopotassium phosphate, and 0.8 mM, disodium phosphate). This solution allowed preventing the diacetylmorphine degradation, as previously described (Hutchinson, 2002). Stocks of 10 mM diacetylmorphine were kept at -20ºC. For the experiments, dilutions of this stock were prepared immediately before use in phosphate buffer, pH 7.4, to prevent the acidification of the cell culture medium.

3.2. Cell culture

SH-SY5Y cells, acquired from the American Type Culture Collection (ATCC, USA), were used as a model to measure telomere length. These cells comprise a human neuroblastoma cell line collected from a metastatic bone marrow of a 4-year old female, having an epithelial morphology and can be used in both undifferentiated and differentiated modes. SH-SY5Y cells are commonly used in neurological studies due to the presence of neurotransmitter receptors/transporters (e.g. cholinergic, adrenergic, and dopaminergic). Of note, only dopaminergic neurons are present in both differentiated and undifferentiated forms. In addition, these cells express tyrosine hydroxylase (TH), an enzyme responsible for catalyzing the conversion of the amino acid L-tyrosine to L-3,4-dihydroxyphenylalanine (L-DOPA), which is a precursor of main important neurotransmitters. They express the DA transporter (DAT), as well as DA Receptor subtype 2 (D2R) and DA Receptor subtype 3 (DR3). Since DA release is triggered by several drugs, these cells represent a suitable model to assess the effects of drugs and evaluate their neurotoxicity to dopaminergic neurons. Adrenergic neurons have to be induced by differentiated methods, like retinoic acid (RA) or phorbol esters, like as 12-O-tetradecanoyl-phorbol-13 acetate (TPA). In the differentiated state, the SH-SY5Y express dopamine-β-hydroxylase (enzyme that converts

DA into noradrenaline) and noradrenaline transporter (NET). SH-SY5Y cell line expresses, in undifferentiated and differentiated forms, two main receptors of cholinergic receptors such as nicotinic acetylcholine receptor (nAChR) and muscarinic acetylcholine receptor (mAChR). The expression of mAChR depends on the method of differentiation used (Kovalevich and Langford, 2013).

SH-SY5Y were selected for this study based on their relatively fast doubling time and on expressing opioid receptors. These cells have a reported population doubling time of 27 hours, thus allowing to achieve a greater number of passages, and possibly reach a state of cellular senescence, in a relatively short period of time (Kovalevich and Langford, 2013). In addition, the SH-SY5Y cell line is known to express the μ- and δ-ORs (Kazmi and Mishra, 1986).

SH-SY5Y cells were routinely cultured in 25 cm^2 or 75 cm^2 flasks with Dulbecco's Modified Eagle's Medium (DMEM) supplemented with 10% FBS and 1% of antibiotic/mycotic solution and incubated at 37ºC in a humidified 5% CO_2 atmosphere. Once they reached approximately 70-80% confluence, cells were detached from the flask by using a 0.25% trypsin/EDTA solution and sub-cultured into new cell culture flasks.

3.3. Cell proliferation

The Sulforhodamine B (SRB) assay, performed as previously described (Alexandre et al., 2020), with slight modifications, was used to assess the changes in proliferation rates of SH-SY5Y cells over time. The SRB is a bright pink colorimetric dye that binds to basic amino acids such as arginine, lysine, and histidine, in cells fixed with 1% acetic acid in methanol. In this method, the absorbance values correlate with the total protein amount, being a reliable indicator of cell proliferation (Papazisis et al., 1997).

For this assay, cells were seeded at 3500 cells/well in a 96-well plate. At 0, 24 and 72 hours, cell culture medium was removed and 50 μL of 1 % acid acetic solution in methanol were added to fixate cells. The plates were then stored at -20ºC overnight. On the following day, the fixation solution was discarded, and the plates allowed to dry on an incubator at 37ºC. Twenty-five microliters of a 0.05 % SRB solution (prepared in methanol) were added to each well and the plates allowed to incubate for 1 hour at 37ºC, protected from light. The unbound dye was removed by several washes with 1 % acetic acid. After drying, the plates were again allowed to dry at 37ºC and the bound SRB solubilized with 100μL of 10mM Tris-base (pH=10.5). Absorbance was read at 540 nm in a Bio-Tek PowerWaveX (Bio-Tek, Winooski, VT, USA) microplate reader, using a 10mM Tris-base solution as blank. Results (percentage of proliferation) were expressed as the percentage of SRB binding relatively to the vehicle-treated cells at 0 h, considered as 100% cell viability.

This procedure was repeated at regular passages after cell splitting either at ratios of 1:3 (faster proliferation, cells passaged more often) and 1:10 (slower proliferation, cells passaged less often) to try to identify the Hayflick limit of these cells, as well as the most suitable method to achieve it faster. Proliferation rates at each passage were then calculated considering the variation in the percentages of proliferation between 0 h and 72 h, according to the following equation:

$$Proliferation\ Rate\ = \frac{(\%\ Proliferation\ at\ 72h - \%Proliferation\ at\ 0h\ )}{(72h - 0h)} \qquad \text{(Equation 1)}$$

3.4. Cell viability

3.4.1. MTT reduction assay

The 3-(4,5-dimethylthiazol-2-yl)-2,5-diphenyltetrazolium bromide (MTT) reduction assay was used, as previously described (Soares et al., 2019), to measure the metabolic activity of SH-SY5Y cells exposed to diacetylmorphine. MTT is a tetrazolium yellow-colored dye, which is reduced to purple formazan crystals by cellular oxidoreductases. The insoluble formazan crystals may be dissolved in the presence of an organic solvent (e.g. DMSO) resulting in a purple-colored solution, whose absorbance correlates with metabolic activity levels (Berridge et al., 2005).

Briefly, SH-SY5Y cells were seeded at 8000 cells/well in a 96-well plate and incubated overnight to allow cell adhesion. The cells were then exposed to diacetylmorphine at 1 nM, 100 nM, 1 μM and 100 μM, for 24 h. Afterward, cell culture medium was removed and 100 μL of a 0.5 mg/mL MTT solution were added and the plate incubated for 1 h at 37ºC in a humidified 5% CO_2 atmosphere. The MTT solution was then aspirated and the formazan crystals dissolved in 100 μL of DMSO. The plates were then placed in an orbital shaker for 15 minutes to further dissolve the crystals. Finally, absorbance was read at 550nm in a Bio-Tek PowerWaveX (Bio-Tek. Winooski, VT, USA). Vehicle (5% phosphate buffer, pH=7.4) and positive (1% Triton X-100) controls were also tested. Results were then expressed as the percentage of metabolic activity relatively to the vehicle control.

3.4.2. Lactate dehydrogenase (LDH) release

Lactate dehydrogenase is a cytosolic enzyme present in most cell types that converts pyruvate into lactate using NADH as a cofactor. When any factor leads to cell lysis due to damage of plasma membrane the LDH is released into the extracellular medium and gives the percentage of dead cells. As such, here we used this method, as previously described (Feio-Azevedo et al., 2017), to assess the effects of heroin cell membrane integrity.

SH-SY5Y cells were seeded at 8000 cells/well in a 96-well plate and incubated overnight, to allow proper cell adhesion. Cells were then incubated with 1 nM, 100 nM, 1 μM and 100 μM heroin, at 37ºC in a humidified 5% CO_2 for 24 hours. At the end of the incubation period, extracellular medium of each well was transferred to another 96-well plate (extracellular LDH). Possible cell debris were removed by centrifugation at 9400× g, for 1 min in an Eppendorf centrifuge (Hamburg, Germany). Fifty microliters of each sample were then mixed with 200 μL of 0.28 mM reduced β-nicotinamide adenine nucleotide (β-NADH, prepared in phosphate buffer, pH 7.4), and the reaction initiated by adding 25 μL of a 0.32 mM pyruvate (prepared in phosphate buffer, pH 7.4) as substrate. The rate of conversion of β-NADH into oxidized nicotinamide adenine nucleotide (NAD+) was then followed spectrophotometrically in a Bio-Tek PowerWaveX (Bio-Tek, Winooski, VT, USA) microplate reader at 340 nm, for 5 min.

LDH leakage was then calculated by dividing the LDH released by the total cellular LDH (considered as the LDH released after killing all cells with 1% Triton X-100), according to the Equation 2:

$$\%\ LDH\ release = \frac{extracellular\ LDH}{Total\ LDH} \times 100 \qquad \text{(Equation 2)}$$

3.5. Quantification of telomere length

3.5.1. Drug exposure conditions

Cells at passage 31 were seeded at 1.5×10^5 cells per well in 6-well plates and cells left to adhere overnight. On the following day, the DNA of cells before the heroin or vehicle treatment (basal controls) was extracted to assess the initial length of telomeres. Heroin was then added to the wells, in duplicate, at two concentrations, 1 nM and 1μM, previously confirmed to be non-cytotoxic by the MTT reduction and LDH release assays. A vehicle (phosphate buffer, pH 7.4) control was also tested. Heroin and vehicle were then added every other day. Once cells reached 80-90% confluence, these were trypsinized (with 0.25 % trypsin) and cells from duplicated pooled into a single cell suspension. Part of this cell's suspension was used to maintain the cell culture by using a 1:3 split ratio and the remainder used for DNA extraction. The drug exposure scheme is summarized in Figure 7.

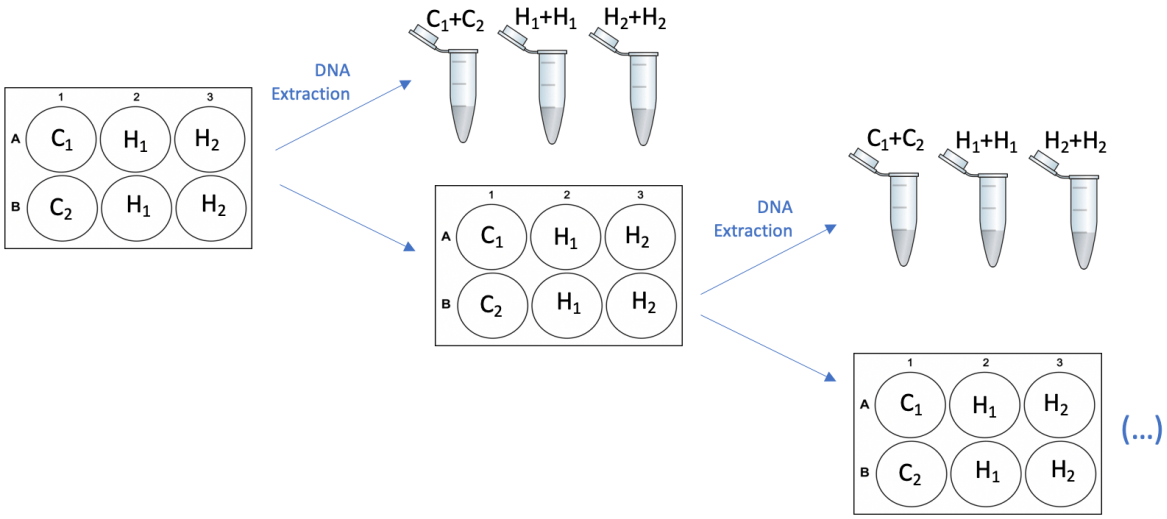

Figure 7. Timeline for heroin treatments. The heroin concentrations were added every other day, 100μM and 1nM, in duplicates, as the controls which the only was treated with the vehicle. After 80-90% reached confluence, trypsinization was used to move to another plate with a split of 1:3, in simultaneous, the extraction of DNA was made.

XAV939 is an inhibitor of tankyrase 1 (TNKS1), which is a positive regulator for telomerase, binding to and stimulating TRF1, thus leading to a decrease in telomeres length. In fact, Tian et al. (2013) have previously shown that 1 μM XAV939 reduced the telomere length of SH-SY5Y cells by inhibiting tankyrase 1 (TNKS1) after 72 hours of exposure, which did neither alter the telomerase activity and did not induce apoptosis. As such, we also exposed SH-SY5Y to this molecule for 72 hours, as a positive control for telomere shortening. Due to XAV939's liposolubility, stocks of 1 mM were prepared in dimethyl sulfoxide (DMSO). At the time of the experiments, XAV939 dilutions were prepared so that the final DMSO concentration in the cell culture medium was not higher than 0.1%. A vehicle (0.1% DMSO) control was also considered. The DNA extraction of XAV939-treated cells was performed at the same day of the first collection of samples treated with heroin, making it possible to compare the telomere length in both conditions at the same time point.

3.6. Genomic DNA extraction

DNA from heroin-, XAV939- or vehicle- treated cells samples was extracted using a commercial genomic DNA extraction kit (Grisp, Porto, Portugal). The method is based on the selective binding of DNA to the glass fiber matrix of the spin columns, following cell lysis and protein denaturation with a chaotropic agent and Proteinase K. Briefly, cells were harvested from the 6-well plates into a falcon of 15 mL and centrifuged at 1000 rpm (Sigma, Germany) for 5 minutes. The supernatant was discarded, and the pellet was resuspended in 200 μL of 1x Phosphate Buffer Saline (PBS) and transferred into a clean 1.5 mL tube. From here, extraction occurred in 4 phases: 1) cell lysis, consisting in lysing the cell

membrane to expose the nuclear DNA, by adding 20 µL of Proteinase K (10 mg/mL), 5 min at 60ºC, to lyse the membranes and denature histones. Two hundred microliters of Buffer BR2 were then added and the tubes incubates for additional 5 min at 60ºC. DNA was precipitated by adding 200 µL of absolute ethanol. 2) DNA binding: DNA was placed in a spin column containing a silica membrane that retains and concentrates the DNA, which in turn was inserted in a 2 mL collection tube. The tube with the spin column was centrifuged at 16,000 g (Sigma, Germany) for 3 min. 3) washing: the collection tube containing the flow-through was discarded and the spin column transferred into a clean 2 mL collection tube. Four hundred microliters of wash buffer 1 were added, and the tubes centrifuged at the same speed (16,000 g) for 1 min, followed by the addition of 600 µL of the wash buffer 2 and new centrifugation at the same conditions as in the previous wash. To dry the matrix of the column, the flow-through was discarded and the tube again centrifuged at the same speed, but for 3 min. 4) DNA elution: the DNA was released from the spin column's membrane with the addition of pre-heated Elution Buffer into the spin column, followed by an incubation for 3 min at room temperature. Afterward, the tubes were centrifuged for 1 minute at the same speed (16,000 g).

The concentration of DNA in each sample was determined in a Qubit™ 4 fluorometer, using the Qubit 1X dsDNA High Sensitivity Assay Kit. At the end of the procedure, the DNA was stored at -20ºC.

3.7. Absolute Telomere length quantification by qPCR

The absolute telomere length in each sample was determined according to the protocol established by Cawthon (Cawthon, 2009) to determine relative telomere length, but modified to introduce an oligomer standard to measure absolute telomere length, as implemented by O'Callaghan and Fenech (O'Callaghan and Fenech, 2011) and later further modified by others (Shalev, 2020). Theoretically, the PCR amplifies DNA exponentially, doubling the number of target molecules with each amplification cycle. In real time PCR, the amount of DNA is measured after each cycle by using fluorescent dyes, being proportional to the amplified DNA amount in the, PCR product.

The procedure used herein gives an approximation of telomeric content per cell (T) by using an 84 bp oligomer standard composed of 14 TTAGGG repeats. The number of the genome copies per sample (S) was also estimated in the same DNA samples by using a second oligomer standard curve to quantify a single-copy gene (SCG). Cawthon (Cawthon, 2009) and O'Callaghan and Fenech (2011) have previously recommended using *36B4* (Acid Ribossomic protein P0, RPL0) as the SCG. Although at the time those protocols were established *36B4* was considered to be a SCG, it has been recently shown that *36B4* is a typical ribosomal gene containing multiple processed pseudogenes in the human genome,

which results on the PCR product giving multiple peaks on the melting curve (Vasilishina et al., 2019). As such, we have also used *IFNB1* (gene coding for interferon beta 1) as the SCG. Of note, *IFNB1* belongs to interferon genes' cluster on chromosome 9 and is represented by single copy in the haploid genome. The oligomers used for the quantification of absolute telomere length are listed in Table 2.

Table 2. Oligomers used for q-PCR.

	Oligomer Name	Oligomer sequence	Amplicon size (bp)
Standards	**Telomere Standard**	5'- $(TTAGGG)_{14}$ -3'	84
	IFNB1	5'- CCTTTCATATGCAGTACATTAGCCATCAGT CACTTAAACAGCATCTGCTGGTTGAAGAAT GCTTGAAGCAATTGTCCAGTCC -3'	82
	36B4	5'- CAGCAAGTGGGAAGGTGTAATCCGTCTCC ACAGACAAGGCCAGGACTCGTTTG TACCCGTTGATGATAGAATGGG- 3'	75
PCR primers	**TeloF**	5'- CGGTTTGTTTGGGTTTGGGTTTGGGTTTG GGTTTGGGTT -3'	84
	TeloR	5'- GGCTTGCCTTACCCTTACCCTTACCC TTACCCTTACCCT- 3'	
	IFNB1F	5'- GGACTGGACAATTGCTTCAAG- 3'	82
	IFNB1R	5'- CCTTTCATATGCAGTACATTAG- 3'	
	36B4F	5'- CAGCAAGTGGGAAGGTGTAATCC -3'	75
	36B4R	5'- CCCATTCTATCATCAACGGGTACAA -3'	

The telomere and the SCG standard curves were generated following the amplification of telomere or SCG standards with a known number of repeats. The Telomere Standard Curve used dilutions ranging from 10^{-1} to 10^{-6}, of a synthesized 84 bp oligonucleotide containing the telomere DNA repeats. The Single Copy Gene Standard was used to determine genome copies per sample and was generated by serial dilutions ranging from 10^{-1} to 10^{-6}. The detailed calculations for the preparation of these solutions are presented in Annex 1.

The correlation coefficient of the standard curve is a measure of how well the data fit the standard curve, thus reflecting its linearity. Moreover, a PCR reaction efficiency of 100 % should equal a slope of -3.32 in the linear regression of the standard curve, according to the equation below:

$$Efficiency = 10^{\left(-\frac{1}{slope}\right)} - 1\ x\ 100 \qquad \text{(Equation 3)}$$

qPCR was performed in a QuantStudio™ 5 Real-Time PCR system (Applied Biosystems, USA) by adding 20 ng (in 4 µL) of DNA from each sample to a reaction mixture containing10 µL of Power SYBR Green master mix (Applied Biosystems, Carlsbad, California, EUA) 1µL of 0.2 µM SCG/Telomere primer forward (final concentration of 0.1 µM), 1µL of 0.2 µM SCG/Telomere primer reverse (final concentration of 0.1 µM), and 4 µL of H_2O. The Power SYBR Green mastermix contains AmpliTAQ Gold DNA polymerase, dNTPs, SYBR I Green Dye, optimized buffers and a passive reference dye. The SYBR Green dye emits a fluorescent signal, which will be detected by the thermal cycler when the dye binds to the double-stranded DNA. The PCR conditions, which were the same for telomeres and SCG amplification were the following: 10 min at 95ºC (DNA denaturation), 40 cycles of 15 sec at 95ºC (annealing), and 60ºC for 1 min (extension), followed by a dissociation curve. All samples were run in triplicate. One negative control (no DNA added), a short telomere control (Jurkat cells' genomic DNA, Thermo Fisher Scientific, Waltham, MA, USA), and a long telomere control (genomic DNA from cell line 1301, Sigma-Aldrich, St. Louis, Missouri), were also tested.

The telomere and SCG standard curves were used to determine absolute telomere length in the unknown samples by interpolation, using the QuantStudio™ Design & Analysis Software v1.4 (Applied Biosystems, USA). The telomeric content per cell (T) was then divided by the number of the genome copies per sample (S) to report the telomeric sequence per cell (T/S). A second division by 96 (considering the existence of 23 chromosomal pairs, included trisomies, a telomere on each end) further indicates telomere length per telomere (in kb values).

3.8. Statistical Analysis

Statistical analysis was performed using GraphPad Prism 8 software (GraphPad Software, La Jolla, CA, USA). Analysis of the normality of each distribution was assessed using the Anderson–Darling, D'Agostino–Pearson and Shapiro–Wilk normality tests, and taking into account the acceptability of skewness and kurtosis values. Based on the normality results,

one-way ANOVA, followed by a Dunnett's post-hoc test were performed. The qPCR data were analyzed by the QuantStudio™ Design & Analysis Software v1.4 (Thermo Fisher Scientific, Waltham, MA, EUA).

4. Results

4.1. Assessment of SH-SY5Y cell proliferation over time

The rate of SH-SY5Y cells' proliferation was followed over several passages to ascertain the passage at which these cells entered the decline in proliferation phase, a stage at which the doubling time is increased, mitotic activity decreases and cell debris start accumulating (Hayflick, 1965). Figure 8A shows the percentage of proliferation obtained for a period of 72 h, assessed using the sulforhodamine B assay, from passage 20 to 33, sub-cultured with split ratios of 1:3. As shown in this figure and further displayed in Fig. 8B, a decrease was noticed between passage 20 and passage 33, being especially evident at higher passages (30 and 33). Passage 21 also showed a statistically significant decrease of the proliferation rate, but this was not maintained after 3 passages, suggesting some inter-passage variability.

Cells were also cultured at a split ratio of 1:10 to assess whether there was any correlation between the beginning of the decline phase and the time spent after the first sub-cultivation (passage), rather than the total number of sub-cultivations. Figure 9A shows the percentage of proliferation of cells at passages 19 and 21. Both this figure and Fig. 9B, which displays the proliferation rates generated from the plot in Fig. 9A show a decreased proliferation rate at passage 19 compared to passage 21. However, due to technical problems it was not possible to obtain data at enough passages with a split ratio of 1:10, so it was not possible to adequately monitor the proliferation rates over time at this split ratio.

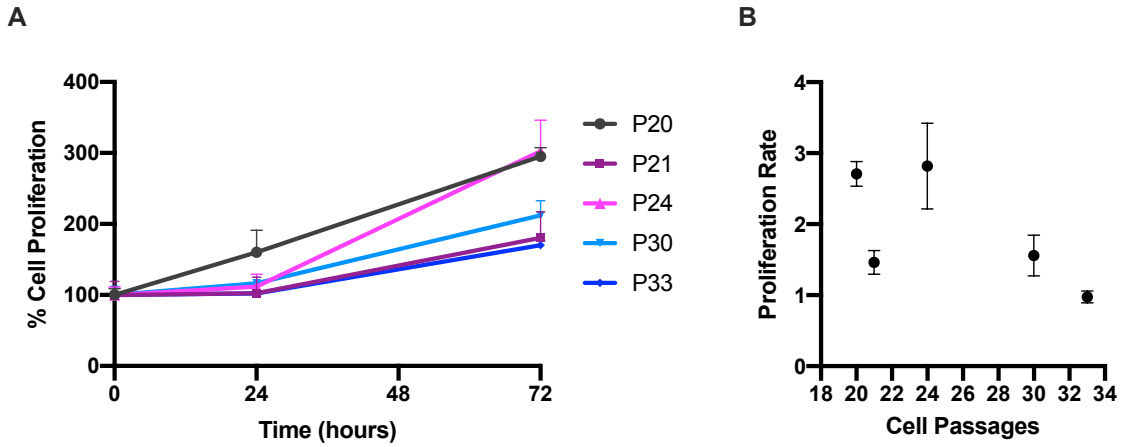

Figure 8. Evaluation of SH-SY5Y cell proliferation after sub-cultivations at a 1:3 split ratio. Cells at passage 20 were split at a ratio of 1:3 once they reached near 80-90 % confluency and this procedure was repeated every time cells reached such confluency up to passage 33. A) At the indicated passages, the percentage of cell proliferation was assessed at three time points (0, 24 and 72 h), using the SRB assay, and compared to the number of cells at day 0 (set as 100 % cell proliferation). B) Proliferation rates, generated from the proliferation curves in Fig. 8A, along the different passages. Data at each point represent the mean ± S.E.M. for three independent experiments, performed in triplicates.

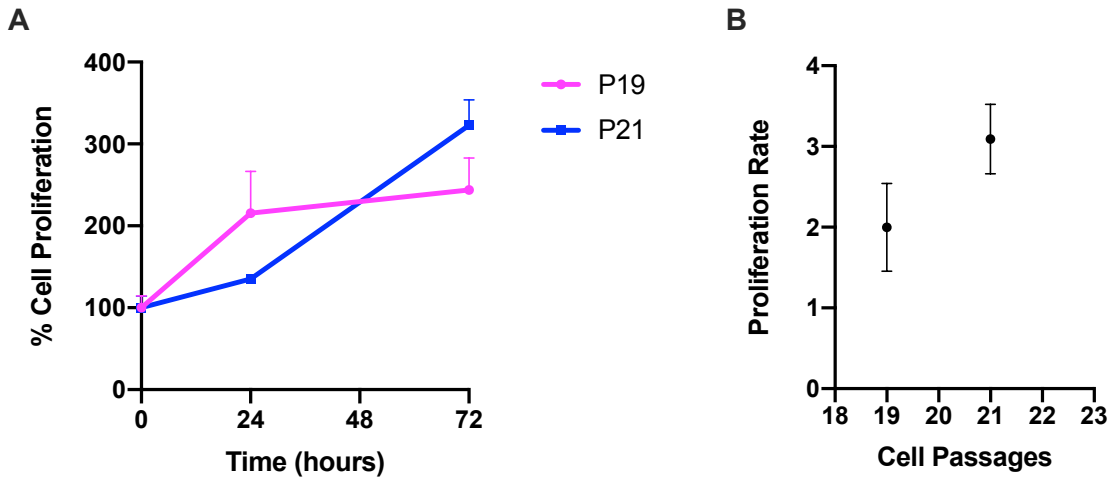

Figure 9. Evaluation of SH-SY5Y cell proliferation after sub-cultivations at a 1:10 split ratio. Cells at passage 19 were split at a ratio of 1:10 once they reached near 80-90 % confluency and this procedure was repeated every time cells reached such confluency. A) At the indicated passages, the percentage of cell proliferation was assessed at three time points (0, 24 and 72 h), using the SRB assay, and compared to the number of cells at day 0 (set as 100 % cell proliferation). B) Proliferation rates, generated from the proliferation curves in Fig. 9A, along the different passages. Data at each point represent the mean ± S.E.M. for three independent experiments, performed in triplicates.

4.2. Determination of cell viability

The toxicity of heroin was measured at a concentration range between 1 nM and 100 μM, by evaluating the heroin's effects in metabolic activity (MTT reduction) and in the cell membrane integrity (LDH release). These parameters were assessed after 24 h of cells' exposure to the four heroin concentrations. Figure 10 shows the assessment of heroin's effects on metabolic activity (Fig. 10A) and on cell membrane integrity (Fig. 10B). As observed in both figures, there are no statistically significant differences for any of the heroin concentrations tested, compared to the vehicle control (phosphate buffer), indicating that heroin does not affect metabolic activity or the disruption of cell membrane up to a concentration of 100 μM.

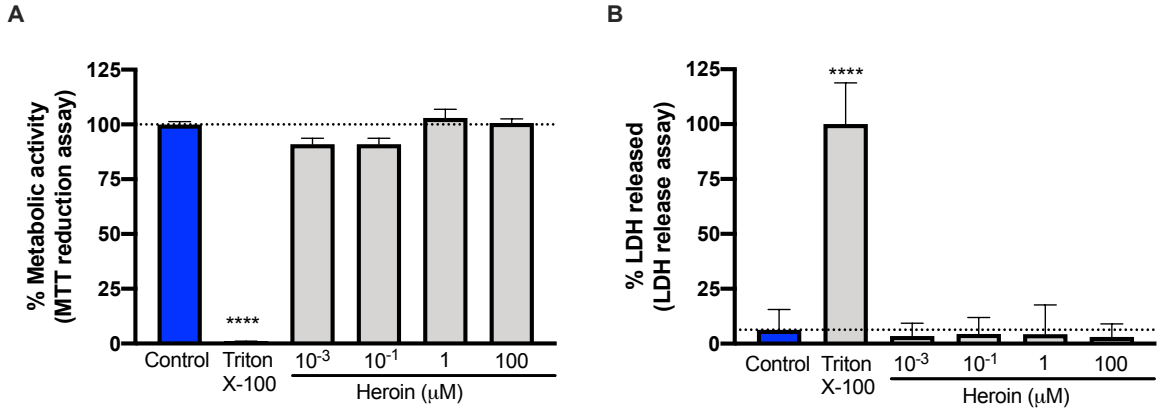

Figure 10. SH-SY5Y cell viability upon heroin exposure. SH-SY5Y cells were seeded in 96-well plates and exposed to four heroin concentrations, ranging from 1 nM to 100 μM, for 24 h. **A)** The percentage of metabolic activity was evaluated by the MTT assay. **B)** Cell membrane integrity was assessed by determining the percentage of LDH release. Each bar represents the mean ± SEM for at least five independent experiments. All samples were run in duplicate. ****p<0.0001, compared to vehicle control (5 % phosphate buffer).

4.3. Evaluation of absolute telomere length by q-PCR

4.3.1. Evaluation of the PCR reaction efficiency

Absolute telomere length was measured using qPCR, according to a previously described method (Cawthon, 2009; O'Callaghan and Fenech, 2011). In this sense, the efficiency of the PCR reaction was firstly determined for all the oligomers used by plotting the log of known amounts of telomeres and single copy genes against the number of Cycle Threshold (Ct).

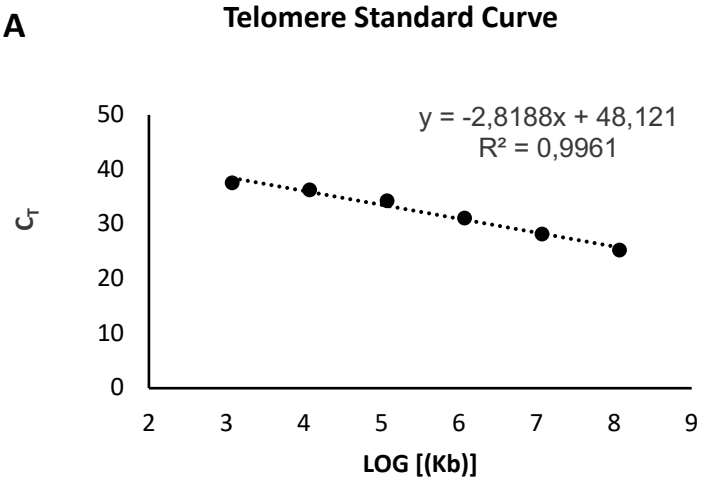

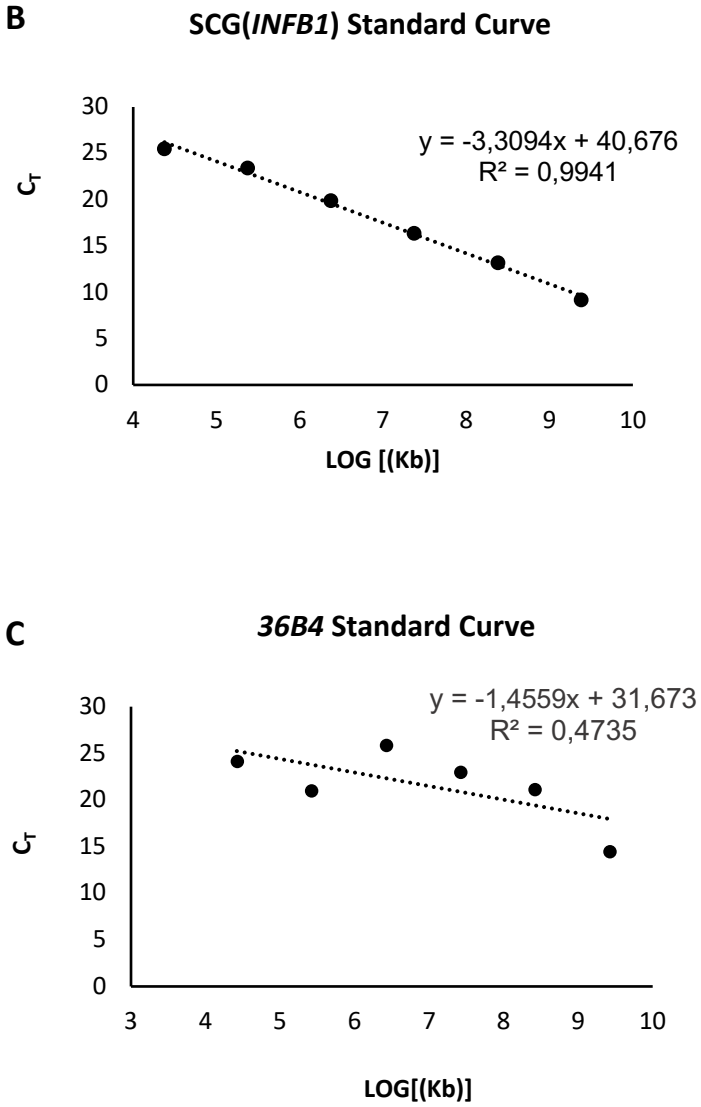

Figure 11. Telomere, and single copy genes (*IFNB1, 36B4*) standard curves. To determine the efficiency of the PCR reactions, the log of known amounts of each oligomer was plotted against the cycle threshold for serial dilutions of: A) an oligomer containing 14 TTAGGG repeats (telomere sequence) (1.18×10^8 and 1.18×10^3 kb). B) an *INFB1* oligomer (2.38×10^9 and $2{,}38 \times 10^4$ kb). The oligomer sequences used are detailed in Materials and Methods. **C)** *36B4* oligomer (2.63×10^9 and 2.63×10^4 kb).

From Fig. 11A it was possible to determine the efficiency, or the PCR reaction related to the amplification of telomere repeats as being 126 % (r^2 = 0.99). The reaction for the *IFNB1* SCG (Fig. 11B) presented an efficiency of 101 % (r^2 = 0.99). However, the reaction for *36B4*, the SCG used in most protocols for the quantification of absolute telomere length (Cawthon, 2009; O'Callaghan and Fenech, 2011) showed a poor efficiency (386 %) and correlation coefficient (r^2 = 0.47). These data are in accordance with recent reports that this

may not be a SCG (Vasilishina et al., 2019). As such, we used *IFNB1* as a SCG to normalize the data concerning the measurement of telomere length.

4.3.2. Evaluation of heroin's effects on absolute telomere length

The possible effects of heroin on telomere length were assessed after 3 and 6 days of every other day exposure to this substance, corresponding to 2 and 3 heroin administrations, respectively. Based on cell proliferation data, cells were split at a 1:3 ratio once they reached 80-90% confluency. Absolute telomere length was then determined by qPCR.

The procedure was validated by using two positive controls: Jurkat cells' genomic DNA, as a control for short telomeres, and genomic DNA from the cell line 1301, recognized for its long telomeres. As observed in Figure 12, there is notorious difference between both, with the method used identifying short telomeres for Jurkat cells and long telomeres for cell line 1301. Fig. 12 further shows that absolute telomere length in the vehicle (phosphate buffer) control 3 days after the beginning of the treatments was very similar to absolute telomere length in the baseline controls (approximately 3436 ± 838 kb/telomere). At the same time point, 1 nM heroin presented a telomere length of 1807 ± 947.6 kb/telomere. However, no statistical differences were found, indicating that this heroin concentration did not have any effect on this parameter, under the present experimental conditions. Also, 1 μM heroin did not alter telomere length, compared to controls 3478 ± 1538 kb/telomere. Due to technical problems, the data for a 6-day treatment is representative of a single independent assay, making it impossible to withdraw any conclusions. XAV939, a tankyrase inhibitor that has already been described to promote telomere shortening in neuroblastoma cells (Tian et al., 2014), was used as a reference. As shown in Fig. 12, exposure of SH-SY5Y cells to 1 μM XAV939 for 72 hours resulted in telomeres with 2168 ± 731 kb/telomere, while telomeres in the respective vehicle control (0.1% DMSO) showed a length of 2986 ± 837 kb/telomere. However, contrarily to what was expected, these values were not significantly different.

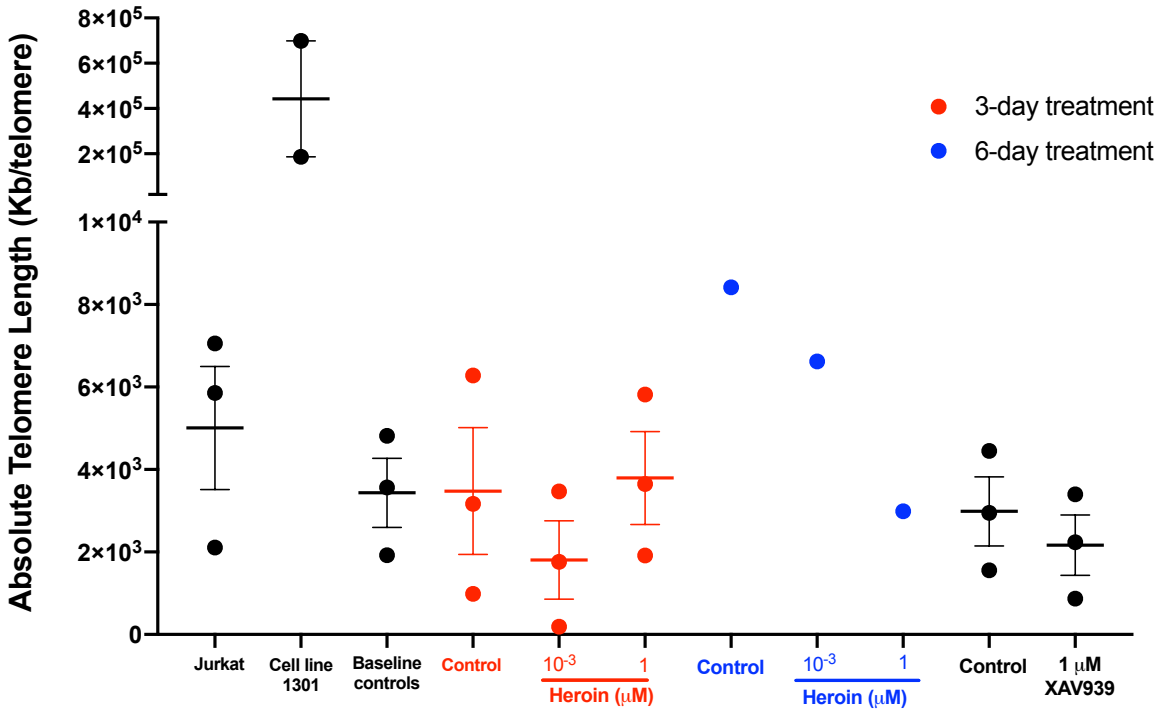

Figure 12. Absolute Telomere length. The heroin treatments were maintained during 6 days in duplicate and with 10^{-3} M and 1μM. The first DNA extraction, at passage 31, was collected after 3 days (red colour), with 2 times heroin administrations and in the control was added of phosphate buffer pH=7). The second DNA extraction were collected at 6 days treatment with 3 times heroin exposure (blue colour) and in this case, only one single experience. The genomic DNA of Jurkat and cell line 1301 were used as positive controls for short and long telomeres, respectively. The baseline controls were DNA collected in day 0, without any treatment, to compare with differences between initial state and the treatments. Each assay condition runs in duplicate, in three independent experiments. The horizontal lines show the mean ± SEM.

5. Discussion

Telomere shortening is a commonly used biomarker for aging. Many signaling pathways are involved in this process that may be influenced by a set of different factors such as everyday habits, lifestyle, diseases, injury, among others (Bachi et al., 2017; Calcinotto et al., 2019). Drug abuse (e.g. alcohol, cocaine, tobacco) has also been associated with premature aging and death (Levandowski et al., 2016; Vakonaki, 2019; Valdes et al., 2005). The effects of heroin on telomere length, especially in neuronal cells, remains unclear, although there seems to be some evidence that telomeres shortening may be a potential consequence of heroin use (Cheng et al., 2013; Yang et al., 2013). In this study we aimed at assessing the effects of heroin on telomere length in the SH-SY5Y cell line.

It is well-established that following a period of active multiplication, cells' mitotic activity starts declining, generation time increases, and cellular debris accumulate, leading to the degeneration of the culture (Hayflick, 1965). Therefore, we primarily tried to determine the number of sub-cultivations required for SH-SY5Y cells cultured at initial passages (presenting regular doubling times) to reach that decline phase, by assessing their proliferation rates at different passages. This would allow us to determine the most adequate time of exposure required to notice any earlier shortening of telomeres upon exposure to heroin, compared to untreated cells. Cells were cultured at split ratios of either 1:3 or 1:10. According to Hayflick (1965), the smaller the split ratio (e.g. 1:3), the more passages are made, making an eventual decreased proliferation visible earlier than for a larger split. Moreover, the use of a larger split ratio (1:10) allows assessing if the time spent after the first sub-cultivation, instead of the total number of sub-cultivations, influenced the passage/time at which cells reached the decline stage. Our data showed a decrease in proliferation rates between passages 20 and 33, suggesting an approximation to the state of cellular senescence. However, it would be important confirm if the proliferation rate at the subsequent passages remained low. Of note, passage 21 also showed a statistically significant decrease of the proliferation rate, but this was not maintained after 3 passages, suggesting some occasional variability in the proliferation of these cells. A similar variability was also observed by Hayflick in WI-26 (male fetal human lung), WI-38 and WI-44 (female human fetal lung) cells (Hayflick, 1965). Considering the longer period for cells at a 1:10 split ratio to reach 80-90% confluence, compared to the 1:3 split ratio, it was not possible to obtain data from enough time points. As such, it was not possible to ascertain if time spent following the first sub-cultivation, rather than the number of sub-cultivations, was sufficient for cells to reach the decline phase.

Our data also showed that heroin did not affect metabolic activity or the integrity of the cell membrane of SH-SY5Y cells up to 100 μM. These results are in accordance with previous studies. For example, Cunha-Oliveira et al. (2007) previously showed that street heroin reduced metabolic activity of cortical neurons after 24 h exposure with IC_{50} and IC_{10} corresponding to about 840 and 215.2 μM heroin, respectively. The authors observed no changes in LDH release, suggesting that heroin did not cause necrotic cell death. Thomas et al. (1995) observed a decreased in B-cell proliferation following these cells' exposure to 1-100 μM heroin concentrations. However, it is important to note that the study was conducted on mice-derived splenic lymphocyte cells and such effects were only noted after 68 h of exposure. Based on our data, we selected 1 nM and 1 μM of heroin to assess the heroin's effects on telomere length.

We firstly assessed the efficiency of the PCR reaction for the telomere and *36B4* oligomers. The sequences of these oligomers were based on the sequences previously described (Cawthon, 2009; O'Callaghan and Fenech, 2011). A good reaction should have an efficiency between 90% and 110%, with an ideal 100 % efficiency meaning that the template doubles after each thermal cycle during exponential amplification. We observed an efficiency slightly higher for the PCR reaction concerning the telomere oligomer, suggesting that there one or more reagents could contain reaction inhibitors. On the other hand, the reaction for *36B4* showed a very low efficiency, which could be attributed to experimental factors that could interfere with the efficacy of the PCR reaction, such as length, formation of secondary structures (e.g. primer-dimers), or reaction dynamics. Moreover, it was recently found that *36B4* is not an SCG, hindering its use in the measurement of the length of the telomeres. In fact, *36B4* is a gene with multiple pseudogenes processed in the human genome, resulting in several peaks in the melting curve, which influences the accuracy of telomere length quantification (Vasilishina et al., 2019). As such, we used *IFNB1* as an SCG instead. *IFNB1* is a gene that codes for a cytokine (Interferon Beta-1) that is released in response to virus and bacterial infections, and cancer (PubMed). *IFNB1* is an SCG in the haploid genome, located on chromosome 9 (Vasilishina et al., 2019). Noteworthy, the PCR reaction for the amplification of this gene showed an efficiency of 101%.

Concerning telomere length, cells cultured at passage 31 and treated with vehicle (phosphate buffer) for 3 days showed a telomere length similar to baseline controls (day 0, without any treatment). Moreover, at this time point, none of the heroin concentrations tested significantly altered telomere length. Surprisingly, SH-SY5Y exposure to 1 μM XAV939 for 72 hours also did not induce statistically significant changes in telomere length, contrasting data previously obtained by Tian et al. (Tian et al., 2014). XAV939 is a molecule that inactivates TNKS1, has been the target of research to control the growth of malignant

cells, leading to apoptosis. Of note, telomerase activity is positively stimulated by TNKS1, thus the action of XAV939 interferes with the extension of the telomere length. (Tian et al., 2014). It should be noted that the data presented only derives from three independent experiments, which could partly explain the elevated standard errors observed. Moreover, this elevated variation in data range was already reported by O'Callaghan and Fenech in their original protocol (O'Callaghan and Fenech, 2011). These authors determined the telomere length in two matrices, lymphocytes and buccal cells. They separated the analysis of telomere length by male and female genders at ages between 18 and 31 (young people group), and compared these results with another group, aged between 65 and 75 years old (older people group). They observed a large variation in the data obtained, regardless of the type of cells analyzed or the age group. For example, in lymphocytes from the young people group, the absolute telomere length had a range of 35-260 kb, and the buccal cells between 45-594 kb. In the older people group, the range of absolute telomere length of lymphocytes is 35-174 kb, and the buccal cells had a range of 33-750 kb (O'Callaghan and Fenech, 2011).

It is also worth noting that in our work the assays aimed at assessing telomere length started in cells at passage 31. Ideally, based on the cell proliferation data, obtained in the meantime, it would likely be more adequate to start heroin administrations at passage 20, for example, since cells at this passage seem to proliferate at a regular pace, and maintain repeated administrations of heroin up to at least passage 33 (since at this stage cells seem to have entered a proliferation decline stage). This would likely allow us to work within a larger variation in the length of telomere, thus facilitating the identification of noticeable changes in telomere length between heroin-treated and non-treated cells. However, due to the lockdown imposed by the Covid-19 pandemic, our laboratory was shut down for 3 months and it was not possible to complete the proliferation assays prior to heroin exposure. In fact, these could only be performed after the lockdown, thus hindering the proper planning of heroin exposure settings.

6. Conclusion and Future Perspectives

In this work, a protocol for the assessment of absolute telomere length was successfully established, as it was possible to determine the length of telomeres following the exposure of SH-SY5Y neuroblastoma cells to two different concentrations of heroin. This assay was validated by the proper identification of short and long telomeres in the genomic DNA of Jurkat cells or cell line 1301, respectively. Our preliminary results point towards a trend of heroin to decrease TL after 3 days exposure, but the data obtained was not entirely clear due to its high variability. However, mainly due to the Covid-19 pandemic-related lockdown, and the further restrictions that applied in laboratory activities, it was not possible to follow our original plan. In this sense, further experimental work is required to clarify the possible involvement of heroin in telomere shortening in neurons.

One of the main limitations in this work concerned the assessment of the Hayflick limit for this cell line. Although our data suggest that at passage 30 the cells' proliferation rate appeared to decline, it would be important to determine such parameter at higher passages. Moreover, considering that telomere shortening is usually described as a slow process, it would be interesting to start heroin's exposure at an earlier cell passage and extend it for a much longer period, to clarify how prolonged cells' exposure to heroin may affect TL. Considering the variability observed in telomere length measured by qPCR, it could also be interesting to support data concerning TL quantification by comparing the results obtained through qPCR with a standard complimentary method, such as the terminal restriction fragment assay. Finally, telomerase activity should be measured in future studies as it is an important factor to consider, to further understand the interaction of heroin with telomere structure and function.

7. References

[1] Alexandre J, Malheiro R, Dias da Silva D, Carmo H, Carvalho F, Silva JP, 2020, "The Synthetic Cannabinoids THJ-2201 and 5F-PB22 Enhance In Vitro CB(1) Receptor-Mediated Neuronal Differentiation at Biologically Relevant Concentrations", Int J Mol, 21(17), 6277.

[2] Arsenis N, C, You T, Ogawa EF, Tinsley GM, Zuo L, 2017, "Physical activity and telomere length- Impact of aging and potential mechanisms of action", Oncotarget, 8, 45008-45019.

[3] Azzalin CM, Lingner J, 2015, "Telomere functions grounding on TERRA firma", Trends Cell Biol, 25(5), 29-36.

[4] Bachi K, Sierra S, Volkow ND, Goldstein RZ, Alia-Klein N, 2017, "Is biological aging accelerated in drug addiction?", Curr Opin Behav Sci, 13, 34-39.

[5] Banta-Green CJ, Coffin PO, Schoeppe JA, Merrill JO, Whiteside LK, Ebersol AK, 2017, "Heroin and pharmaceutical opioid overdose events: Emergency medical response characteristics", Drug Alcohol Dependm, 178, 1-6.

[6] Barke KE, Hough LB, 1993, "Opiates, mast cells and histamine release", Life Sci, 53(18), 1391-9.

[7] Barnes RP, Fouquerel E, Opresko PL, 2019, "The impact of oxidative DNA damage and stress on telomere homeostasis", Mech Ageing Dev, 177, 37-45.

[8] Barrio G, Montanari L, Bravo MJ, Guarita B, Fuente L, Pulido J, Vicente J, 2013, "Trends of heroin use and heroin injection epidemics in Europe: findings from the EMCDDA treatment demand indicator (TDI)", J Subst Abuse Treat, 45(1), 19-30.

[9] Bateson M, Aviv A, Bendix L, Benetos A, Ben-Shlomo Y, Bojesen SE, Cooper C, Cooper R, Deary IJ, Hägg S, Harris SE, Kark JD, Kronenberg F, Kuh D, Labat C, Martin-Ruiz CM, Meyer C, Nordestgaard BG, Penninx BWJH, Pepper GV, Révész D, Said MA, Starr JM, Syddall H, Thomson WM, Harst Pvd, Whooley M, Zglinicki Tv, Willeit P, Zhan Y, Nettle D, 2019, "Smoking does not accelerate leucocyte telomere attrition: a meta-analysis of 18 longitudinal cohorts", R. Soc. Open Sci., 6(6), 190420.

[10] Berridge MV, Herst PM, Tan AS, 2005, "Tetrazolium dyes as tools in cell biology: new insights into their cellular reduction", Biotechnol Annu Rev, 11, 127-52.

[11] Buttner A, Malla, G, Penninga, R, Weisb S, 2000, "The neuropathology of heroin abuse", Forensic Sci. Int.,113, 435-442.

[12] Calcinotto A, Kohli J, Zagato E, Pellegrini L, Demaria M, Alimonti A, 2019, "Cellular Senescence: Aging, Cancer, and Injury", Physiol Rev, 99(2), 1047-1078.

[13] Campa D, Matarazzi M, Greenhalf W, Bijlsma M, Saum K-U, Pasquali C, van Laarhoven H, Szentesi A, Federici F, Vodicka P, Funel N, Pezzilli R, Bueno-de-Mesquita HB, Vodickova L, Basso D, Obazee O, Hackert T, Soucek P, Cuk K, Kaiser J, Sperti C, Lovecek M, Capurso G, Mohelnikova-Duchonova B, Khaw K-T, König A-K, Kupcinskas J, Kaaks R, Bambi F, Archibugi L, Mambrini A, Cavestro GM, Landi S, Hegyi P, Izbicki JR, Gioffreda D, Zambon CF, Tavano F, Talar-Wojnarowska R, Jamroziak K, Key TJ, Fave GD, Strobel O, Jonaitis L, Andriulli A, Lawlor RT, Pirozzi F, Katzke V, Valsuani C, Vashist YK, Brenner H, Canzian F, 2019, "Genetic determinants of telomere length and risk of pancreatic cancer: a pandora study", Int J Cancer, 144, 1275-1283.

[14] Canela A, Vera E, Klatt P, Blasco MA, 2007, "High-throughput telomere length quantification by FISH and its application to human population studies", Proc Natl Acad Sci U S A, 104(13), 5300-5.

[15] Carvalho LM, Wiers CE, Manza P, Sun H, Schwandt M, Wang G-J, Grassi-Oliveira R, Godard ALB, Volkow ND, 2019, "Effect of alcohol use disorder on cellular aging", Psychopharmacology, 236(11), 3245-3255.

[16] Cawthon RM, 2009, “Telomere length measurement by a novel monochrome multiplex quantitative PCR method”, Nucleic Acids Res, 37(3), e21.

[17] Cheng GL, Zeng H, Leung MK, Zhang HJ, Lau BW, Liu YP, Liu GX, Sham PC, Chan CC, So KF, Lee TM, 2013, “Heroin abuse accelerates biological aging: a novel insight from telomerase and brain imaging interaction”, Transl Psychiatry, 3, e260.

[18] Christie MJ, 2008, “Cellular neuroadaptations to chronic opioids: tolerance, withdrawal and addiction”, Br J Pharmacol, 154(2), 384-96.

[19] Corder G, Castro DC, Bruchas MR, Scherrer G, 2018, “Endogenous and Exogenous Opioids in Pain”, Annu Rev Neurosci, 41, 453-473.

[20] Cunha-Oliveira T, Rego AC, Garrido J, Borges F, Macedo T, Oliveira CR, 2007, “Street heroin induces mitochondrial dysfunction and apoptosis in rat cortical neurons”, J. Neurochem., 101(2), 543-554.

[21] Del Vecchio G, Spahn V, Stein C, 2017, “Novel Opioid Analgesics and Side Effects”, ACS Chem. Neurosci., 8(8), 1638-1640.

[22] Dinis-Oliveira RJ, 2019, “Metabolism and metabolomics of opiates: A long way of forensic implications to unravel”, J Forensic Leg Med, 61, 128-140.

[23] Drewes AM, Jensen RD, Nielsen LM, Droney J, Christrup LL, Arendt-Nielsen L, Riley J, Dahan A, 2013, “Differences between opioids: pharmacological, experimental, clinical and economical perspectives”, Br J Clin Pharmacol, 75(1), 60-78.

[24] Emery MA, Akil H, 2020, “Endogenous Opioids at the Intersection of Opioid Addiction, Pain, and Depression: The Search for a Precision Medicine Approach”, Annu Rev Neurosci, 355-374.

[25] European Monitoring Centre for Drugs and Drugs Addiction(EMCDDA), 2019, “European Drug Report: Trends and Developments”, EMCDDA.

[26] European Monitoring Centre for Drugs and Drugs Addiction(EMCDDA), 2019, “Portugal Country Drug Report 2019”, EMCDDA, 1-31.

[27] Farmer AD, Holt CB, Downes TJ, Ruggeri E, Del Vecchio S, De Giorgio R, 2018, “Pathophysiology, diagnosis, and management of opioid-induced constipation”, Lancet Gastroenterol Hepatol, 3(3), 203-212.

[28] Fathi E, Charoudeh HN, Sanaat Z, Farahzadi R, 2019, “Telomere shortening as a hallmark of stem cell senescence”, Stem Cell Investig, 6, 7.

[29] Feio-Azevedo R, Costa VM, Ferreira LM, Branco PS, Pereira FC, Bastos ML, Carvalho F, Capela JP, 2017, “Toxicity of the amphetamine metabolites 4-hydroxyamphetamine and 4-hydroxynorephedrine in human dopaminergic differentiated SH-SY5Y cells”, Toxicol Lett, 269, 65-76.

[30] Feltenstein MW, See RE, 2008, “The neurocircuitry of addiction: an overview”, Br J Pharmacol 154(2), 261-74.

[31] Frohnert BI, Sinaiko AR, Serrot FJ, Foncea RE, Moran A, Ikramuddin S, Choudry U, Bernlohr DA, 2011, “Increased Adipose Protein Carbonylation in Human Obesity”, Obesity, 19(9), 1735-1741.

[32] Gardner EL, 2011, “Addiction and brain reward and antireward pathways”, Adv Psychosom Med, 30, 22-60.

[33] Giardini MA, Segatto M, Silva MS, Nunes VS, Cano MI, 2014, “Telomere and telomerase biology”, Prog Mol Biol Transl Sci, 125, 1-40.

[34] Gottås A, Øiestad EL, Boix F, Vindenes V, Ripel Å, Thaulow CH, Mørland J, 2013, “Levels of heroin and its metabolites in blood and brain extracellular fluid after i.v. heroin administration to freely moving rats”, Br J Pharmacol, 170(3), 546-556.

[35] Grun LK, Teixeira NDR, Jr, Mengden LV, de Bastiani MA, Parisi MM, Bortolin R, Lavandoski P, Pierdona V, Alves LB, Moreira JCF, Mottin CC, Jones MH, Klamt F, Padoin AV, Guma FCR, Barbe-Tuana FM, 2018, “TRF1 as a major contributor for telomeres' shortening in the context of obesity”, Free Radic Biol Med, 129, 286-295.

[36] Gutowicz M, Sadurska B, Cholojczyk M, Pokorska-Lis M, Siwinska-Ziolkowska A, Baranczyk-Kuzma A, 2006, “Antioxidant status in different regions of heroin addicts' brain”, Environ Toxicol Pharmacol, 21(1), 80-5.

[37] Hayflick L, 1965, “The limited in vitro lifetime of human diploid cell strains”, Exp. Cell Res., 37, 614-636

[38] Hemann MT, Strong MA, Hao L-Y, Greider CW, 2001, “The Shortest Telomere, Not Average Telomere Length, Is Critical for Cell Viability and Chromosome Stability”, Cell, 107(1), 67-77.

[39] Hirota KS, K S, Lambert DG, 1999, “Interaction of ketamine with μ2 opioid receptors in SH-SY5Y human neuroblastoma cells”, J. Anesth., 13, 107-109.

[40] Hutchinson MR, Somogyi AA, 2002, “Diacetylmorphine degradation to 6-monoacetylmorphine and morphine in cell culture - implications for in vitro studies”, Eur J Pharmacol, 453, 27-32.

[41] Kazmi SMI, Mishra RK, 1986, “Opioid receptors in human neuroblastoma SH-SY5Y cells: Evidence for distinct morphine (μ) and enkephalin (δ) binding sites”, Biochem Biophys Res Commun, 137(2), 813-820.

[42] Khan RJ, Gebreab SY, Gaye A, Crespo PR, Xu R, Davis SK, 2019, “Associations of smoking indicators and cotinine levels with telomere length: National Health and Nutrition Examination Survey”, Prev Med Rep, 15, 100895.

[43] Kiyatkin EA, 2019, “Respiratory depression and brain hypoxia induced by opioid drugs: Morphine, oxycodone, heroin, and fentanyl”, Neuropharmacology, 151, 219-226.

[44] Kolodny A, Courtwright DT, Hwang CS, Kreiner P, Eadie JL, Clark TW, Alexander GC, 2015, “The Prescription Opioid and Heroin Crisis: A Public Health Approach to an Epidemic of Addiction”, Annu. Rev . Public Health, 36(1), 559-574.

[45] Kosten TR, George TP, 2002, “The neurobiology of opioid dependence: implications for treatment”, Sci Pract Perspect, 1(1), 13-20.

[46] Kovalevich J, Langford D, 2013, “Considerations for the use of SH-SY5Y neuroblastoma cells in neurobiology”, Methods Mol Biol, 1078, 9-21.

[47] Lab S, 2020, “Telomere Length Measurement using QPCR”, Shalev lab.

[48] Lai TP, Wright WE, Shay JW, 2018, “Comparison of telomere length measurement methods”, Philos Trans R Soc Lond B Biol Sci, 373.

[49] Lai TP, Zhang N, Noh J, Mender I, Tedone E, Huang E, Wright WE, Danuser G, Shay JW, 2017, “A method for measuring the distribution of the shortest telomeres in cells and tissues”, Nat Commun, 8(1), 1356.

[50] Levandowski ML, Tractenberg SG, de Azeredo LA, De Nardi T, Rovaris DL, Bau CH, Rizzo LB, Maurya PK, Brietzke E, Tyrka AR, Grassi-Oliveira R, 2016, “Crack cocaine addiction, early life stress and accelerated cellular aging among women”, Prog Neuropsychopharmacol Biol Psychiatry, 71, 83-9.

[51] Liu MY, Nemes A, Zhou QG, 2018, “The Emerging Roles for Telomerase in the Central Nervous System”, Front Mol Neurosci, 11, 160.

[52] López-Flores LA, Pérez-Rubio G, Falfán-Valencia R, 2017, “Distribution of polymorphic variants of CYP2A6 and their involvement in nicotine addiction”, EXCLI J 16, 174-196.

[53] Lu W, Zhang Y, Liu D, Songyang Z, Wan M, 2013, “Telomeres-structure, function, and regulation”, Exp Cell Res, 319(2), 133-41.

[54] Luethi D, Liechti ME, 2020, “Designer drugs: mechanism of action and adverse effects”, Arch Toxicol, 94(4), 1085-1133.

[55] Magalhães JP, Passos JF, 2018, “Stress, cell senescence and organismal ageing”, Mech Ageing Dev, 170, 2-9.

[56] Manzke T, Guenther U, Ponimaskin EG, Haller M, Dutschmann M, Schwarzacher S, Richter DW, 2003, “5-HT4(a) receptors avert opioid-induced breathing depression without loss

[57] Martinez MA, Ballesteros S, 2019, Opium poisoning in modern times. An overview, Forensic Sci Int, 302, 109848.

[58] Martinez P, Blasco MA, 2015, “Replicating through telomeres: a means to an end”, Trends Biochem Sci, 40(9), 504-15.

[59] Medicurio, 2018, Opioid Drugs, Part 1: Mechanism of Action, https://www.youtube.com/watch?v=s60KzN4GJdQ, (acessed: 14/04/2020).

[60] Mender I, Shay JW, 2015, “Telomere Restriction Fragment (TRF) Analysis”. Bio Protoc, 5(22).

[61] Miller AD, Leslie RA, 1994, “The area postrema and vomiting”, Front Neuroendocrinol, 15(4), 301-20.

[62] Moreno-Rius J, 2019, “Opioid addiction and the cerebellum”, Neurosci Biobehav Rev, 107, 238-251.

[63] Muhuri MK, Gfroerer JC, Davies MC, 2013, “Associations of Nonmedical Pain Reliever Use and Initiation of Heroin Use in the United States”, Journal CBHSQ, 1-17.

[64] O'Callaghan NJ, Fenech M, 2011, “A quantitative PCR method for measuring absolute telomere length”, Biol Proced Online, 13, 3.

[65] Papazisis KT, Geromichalos GD, Dimitriadis KA, Kortsaris AH, 1997, “Optimization of the sulforhodamine B colorimetric assay”, J Immunol Methods 208(2), 151-158.

[66] PubMed, “IFNB1 interferon beta 1 [Homo sapiens (human)]”, https://www.ncbi.nlm.nih.gov/gene?Db=gene&Cmd=ShowDetailView&TermToSearch=3456 , (accessed 08/10/2020).

[67] Rook EJ, Huitema ADR, Brink W, Ree JM, Beijnen JH, 2006, “Pharmacokinetics and Pharmacokinetic Variability of Heroin and its Metabolites: Review of the Literature”, Curr. Clin. Pharmacol.,109-118.

[68] Roxburgh A, Hall WD, Gisev N, Degenhardt L, 2019, “Characteristics and circumstances of heroin and pharmaceutical opioid overdose deaths: Comparison across opioids”, Drug Alcohol Depend, 205, 107533.

[69] Sato T, Sakuta Y, Suzuki J, Takaku A, 1979, “Successful surgical treatment of intracranial mycotic aneurysm with brain abscess - Report of a case”, Acta Neurochir (Wien), 47(1-2), 53-61.

[70] Savale L, Chaouat A, Bastuji-Garin S, Marcos E, Boyer L, Maitre B, Sarni M, Housset B, Weitzenblum E, Matrat M, Le Corvoisier P, Rideau D, Boczkowski J, Dubois-Randé J-L, Chouaid C, Adnot S, 2009, “Shortened telomeres in circulating leukocytes of patients with chronic obstructive pulmonary disease”, Am J Respir Crit Care Med, 179(7), 566-571.

[71] Savolainen K, Eriksson JG, Kajantie E, Lahti M, Räikkönen K, 2014, “The history of sleep apnea is associated with shorter leukocyte telomere length: the Helsinki Birth Cohort Study”, Sleep Med, 15(2), 209-212.

[72] Schaefer CP, Tome ME, Davis TP, 2017, “The opioid epidemic: a central role for the blood brain barrier in opioid analgesia and abuse”, Fluids Barriers CNS,14(1), 32.

[73] Shay JW, Wright WE, 2019, “Telomeres and telomerase: three decades of progress”, Nat. Rev. Genet., 20, 299-309.

[74] Shirley Y. Hill, PH.D, Michael A. Mikhael, M.D, 1979, “Computerized Transaxial Tomographic and Neuropsychological Evaluations in Chronic Alcoholics and Heroin Abusers”, Am J Psychiatry, 136(4B), 598-602.

[75] Soares J, Costa VM, Gaspar H, Santos S, de Lourdes Bastos M, Carvalho F, Capela JP, 2019, “Structure-cytotoxicity relationship profile of 13 synthetic cathinones in differentiated human SH-SY5Y neuronal cells”, Neurotoxicology, 75, 158-173.

[76] Solis E Jr, Cameron-Burr KT, Kiyatkin EA, 2017, “Heroin Contaminated with Fentanyl Dramatically Enhances Brain Hypoxia and Induces Brain Hypothermia”, eNeuro, 4(5), 1-10.

[77] Solis E, Cameron-Burr KT, Shaham Y, Kiyatkin EA, 2018, “Fentanyl-Induced Brain Hypoxia Triggers Brain Hyperglycemia and Biphasic Changes in Brain Temperature”, Neuropsychopharmacology, 43(4), 810-819.

[78] Songyang Z, 2017, “Telomeres and Telomerase”, Springer Science, XI, 218.

[79] Srinivas N, Rachakonda S, Kumar R, 2020, “Telomeres and Telomere Length: A General Overview”, Cancers, 12(3), 558.

[80] Stein C, 2016, Opioid Receptors, Annu Rev Med, 67, 433-51.

[81] Stout SA, Lin J, Hernandez N, Davis EP, Blackburn E, Carroll JE, Glynn LM, 2017, “Validation of Minimally-Invasive Sample Collection Methods for Measurement of Telomere Length”, Front Aging Neurosci, 9, 397.

[82] Thaulow CH, Øiestad Å ML, Rogde S, Andersen JM, Høiseth G, Handal M, Mørland J, Vindenes V, 2018, “Can measurements of heroin metabolites in post-mortem matrices other than peripheral blood indicate if death was rapid or delayed?”, Forensic Sci Int, 290, 121-128.

[83] Thomas ET, House RV, Bhargava H, 1995, “Direct Cellular Immunomodulation Produced by Diacetylmorphine (Heroin) or Methadone”, Gen. Pharmac., 26, 123-130.

[84] Tian X, Hou W, Bai S, Fan J, Tong H, Bai Y, 2014, “XAV939 promotes apoptosis in a neuroblastoma cell line via telomere shortening”, Oncol Rep, 32(5), 1999-2006.

[85] Tian XH, Hou WJ, Fang Y, Fan J, Tong H, Bai SL, Chen Q, Xu H, Li Y, 2013, “XAV939, a tankyrase 1 inhibitior, promotes cell apoptosis in neuroblastoma cell lines by inhibiting Wnt/β-catenin signaling pathway”, J Exp Clin Cancer Res, 32(1), 100.

[86] Trescot AM, Datta S, Lee M, Hansen H, 2008, “Opioid pharmacology”, Pain Physician, 11(2), S133-53.

[87] United Nations Office on Drugs and Crime(UNODC), 2019, “World Drug Report, United Nations Office on Drugs and Crime”, E.19.XI.8, 1-77.

[88] Vakonaki E, Tzatzarakis M, Tsiminikaki K, Nathena D, Fragkiadaki P, Kalliantasi K, Kanaki K, Vaki G, Plaitis S, Tsoukalas D, Alegakis A, Spandidos DA, Tsatsakis A, 2019, “Effect of chronic and heavy drug abuse on biological aging”, World Acad Sci Eng Technol, 1.2, 67-73.

[89] Valdes AM, Andrew T, Gardner JP, Kimura M, Oelsner E, Cherkas LF, Aviv A, Spector TD, 2005, “Obesity, cigarette smoking, and telomere length in women”, Lancet, 366(9486), 662-4.

[90] Vasilishina, A. Kropotov, I. Spivak, and A. Bernadotte, 2019, "Relative Human Telomere Length Quantification by Real-Time PCR", Cellular Senescence: Methods and Protocols, M. Demaria Ed. New York, NY: Springer New York, pp. 39-44.

[91] Victorelli S, Passos JF, 2017, “Telomeres and Cell Senescence - Size Matters Not”, EBioMedicine, 21, 14-20.

[92] Volkow ND, Michaelides M, Baler R, 2019, “The Neuroscience of Drug Reward and Addiction”, Physiol Rev, 99(4), 2115-2140.

[93] Wandel C, Kim R, Wood M, Wood A, 2002, “Interaction of morphine, fentanyl, sufentanil, alfentanil, and loperamide with the efflux drug transporter P-glycoprotein”, Anesthesiology, 96(4), 913-20.

[94] Wang SG, Hoyte C, 2019, “Novel Drugs of Abuse, Pediatr Rev, 40(2), 71-80.

[95] Weis WI, Kobilka BK, 2018, “The Molecular Basis of G Protein-Coupled Receptor Activation”, Annu Rev Biochem, 87, 897-919.

[96] Williams JT, Christie MJ, Manzoni O, 2001, “Cellular and Synaptic Adaptations Mediating Opioid Dependence”, Physiol. Rev., 81(1), 299-343.

[97] Yamaki N, Matsushita S, Hara S, Yokoyama A, Hishimoto A, Higuchi S, 2019, “Telomere shortening in alcohol dependence: Roles of alcohol and acetaldehyde”, J. Psychiatr. Res., 109, 27-32.

[98] Yang Z, Ye J, Li C, Zhou D, Shen Q, Wu J, Cao L, Wang T, Cui D, He S, Qi G, He L, Liu Y, 2013, “Drug addiction is associated with leukocyte telomere length”, Sci Rep, 3, 1542.

[99] Zhang T, Zheng X, Kim K, Zheng F, Zhan C-G, 2018, “Blocking drug activation as a therapeutic strategy to attenuate acute toxicity and physiological effects of heroin”, Sci. Rep., 8(1), 16762.

[100] Zollner C, Stein C, 2007, “Opioids”, Handb Exp Pharmacol, 177, 231-63.

8. Annex 1

Calculations for the telomere and single copy gene (*IFNB1*) standard curves:

1. Telomere Standard Curve

$\mathbf{MW = 26667,2\ g/mol}$**, Oligomer length: 84 bp**

One molecule weigh:

$$\frac{MW}{Avogadro's\ number} = \frac{26667,2}{6,02 \times 10^{23}} = 0,44\ \times 10^{-19} g$$

Telomere Standard A (highest number of repeats): $60 \times 10^{-12} g$ (per reaction)

To determine the number of molecules of oligomer in a TEL STD A:

$\frac{60 \times 10^{-12} g}{0,44 \times 10^{-19} g} = 1.36\ \times 10^{9}$ molecules

Quantity of telomere sequence in TEL STD A:

$1.36\ \times 10^{9}\ \times\ 84$ oligomer length $= 1.18\ \times 10^{8} Kb$ *of* telemore sequence of TEL STD A

$1.18\ \times 10^{8}\ to\ 1.18\ \times 10^{3}$ dilutions

2. SCG Standard Curve (*IFNB1*)

$\mathbf{MW = 25374,4\ g/mol}$**, Primer length: 82 bp**

One molecule weigh:

$$\frac{MW}{Avogadro's\ number} = \frac{25374,4}{6,02 \times 10^{23}} = 4,21\ \times 10^{-20} g$$

SCG Standard A (SCG STD A) (heavier one):

$200 \times 10^{-12} g$ (per reaction)

To determinate the number of molecules of oligomer in a SCG STD A:

$\frac{200 \times 10^{-12} g}{0,44 \times 10^{-19} g} = 4,751 \times 10^{9}$ molecules

Quantity of *INFB1* sequence in SCG STD A:

The SCG have two copies per diploid gene, thus $\frac{4,751 \times 10^{9}}{2} = 2.3753 \times 10^{9}$

$2.3753 \times 10^{9}\ to\ 2.3753 \times 10^{4}$ dilutions